



RESEARCH ARTICLE

10.1029/2022JG006863

Key Points:

- Wetland tidal creek dissolved organic carbon (DOC) concentration peaked in summer, but monthly estimates of DOC export peaked in early fall
- A lateral export of 200.66 (± 28.09) g C m⁻² years⁻¹ was calculated from the wetland to sub-estuary based on a dataset of over one thousand tidal cycles
- Continuous monitoring improves lateral flux estimates by capturing the variability in water flow and influences by precipitation and wind

Correspondence to:

M. Tzortziou,
mtzortziou@ccny.cuny.edu

Citation:

Menendez, A., Tzortziou, M., Neale, P., Megonigal, P., Powers, L., Schmitt-Kopplin, P., & Gonsior, M. (2022). Strong dynamics in tidal marsh DOC export in response to natural cycles and episodic events from continuous monitoring. *Journal of Geophysical Research: Biogeosciences*, 127, e2022JG006863. <https://doi.org/10.1029/2022JG006863>

Received 16 FEB 2022

Accepted 7 JUN 2022

Author Contributions:

Conceptualization: Alana Menendez, Maria Tzortziou, Patrick Neale, Patrick Megonigal

Formal analysis: Alana Menendez, Maria Tzortziou, Patrick Neale, Leanne Powers, Philippe Schmitt-Kopplin, Michael Gonsior

Funding acquisition: Maria Tzortziou

Investigation: Alana Menendez, Maria Tzortziou, Patrick Neale, Patrick Megonigal

Methodology: Alana Menendez, Maria Tzortziou, Patrick Neale, Patrick Megonigal, Leanne Powers, Michael Gonsior

Strong Dynamics in Tidal Marsh DOC Export in Response to Natural Cycles and Episodic Events From Continuous Monitoring

Alana Menendez^{1,2} , Maria Tzortziou^{1,2} , Patrick Neale³, Patrick Megonigal³, Leanne Powers⁴ , Philippe Schmitt-Kopplin⁵, and Michael Gonsior⁶

¹Earth and Environmental Sciences Program, The City University of New York Graduate Center, New York, NY, USA, ²Department of Earth and Atmospheric Sciences, City University of New York City College, New York, NY, USA, ³Smithsonian Environmental Research Center, Edgewater, MD, USA, ⁴Department of Chemistry, College of Environmental Science and Forestry, State University of New York, Syracuse, NY, USA, ⁵Analytical Biogeochemistry, German Research Center for Environmental Health, Neuherberg, Germany, ⁶Chesapeake Biological Laboratory, University of Maryland Center for Environmental Science, Solomons, MD, USA

Abstract The role of tidal wetlands as hotspots for carbon and nutrient exchange with adjacent waters has been well documented, but large uncertainties remain regarding the physical and biogeochemical controls on these fluxes, which have significant implications for coastal carbon cycling and budgets. This study elucidates the variability in lateral wetland dissolved organic (DOC) fluxes tidally, seasonally, and during extreme weather events for a brackish wetland within a sub-estuary of the northwestern Chesapeake Bay, USA. Continuous fluxes from the wetland-draining tidal creek were calculated based on DOC concentrations ([DOC]) estimated using optical and physicochemical properties measured in situ with concurrent water flow data. Mean export was found to be 8.59 (± 1.20) kg C ($n = 1,128$) tidal cycle⁻¹ and annual flux from the wetland to sub-estuary was 200.66 (± 28.09) g C m⁻² yr⁻¹. Peaks in DOC flux were associated with Hurricane Joaquin in 2015, where just two tidal cycles accounted for ~5% of annual export. Analysis of tidal creek water quality measurements reveal seasonal and tidal dependencies. Highest [DOC] and largest low versus high tide differences were observed in summer, corresponding to more fresh plant biomass and its mobilization, consistent with results from Fourier transform ion cyclotron resonance mass spectrometry. Despite summer highs in tidal creek [DOC], monthly DOC fluxes were greatest in early fall due to higher water flows. The annual flux presented here is higher than fluxes previously reported for this system, highlighting the importance of continuous measurements for monitoring carbon export under a wide range of environmental conditions.

Plain Language Summary Tidal wetlands store a lot of carbon because they have a high input of decaying plant material and typically low oxygen soils, slowing down the breakdown of organic matter. Along the terrestrial-aquatic interface, tidal wetlands continuously exchange dissolved organic carbon (DOC) with adjacent estuarine waters. Here, we wanted to better quantify DOC export with tidal flushing and determine variability with tides, seasons, and storms for a marsh system along the northwestern Chesapeake Bay, USA. To study continuous marsh-estuary exchange, tidal creek DOC concentrations were estimated by developing a strong relationship between laboratory measured DOC and water quality parameters recorded autonomously from an instrument within the creek. DOC flux was calculated by multiplying estimated DOC amount with synchronous water flow measurements, including water volume, speed, and direction. While DOC peaked in the summer when the wetland was the most productive (greenest vegetation and warmest temperature), estimated monthly DOC export was greatest in early fall during highest water flows. The highest fluxes occurred during Hurricane Joaquin because of precipitation and wind direction influences. The annual flux we calculated is higher than values previously published for this wetland, which highlights the need for continuous monitoring to accurately determine carbon exchanges along coasts.

1. Introduction

Human-induced climate change, caused primarily by increasing atmospheric carbon dioxide (CO₂) concentrations, provides an impetus for improvements in global carbon accounting. A major challenge to doing so is accurately distinguishing anthropogenic perturbations from natural carbon fluxes (Regnier et al., 2013). Across the terrestrial-aquatic interface, estuaries are biogeochemical *hot spots*, where critical carbon exchanges and

© 2022 The Authors.

This is an open access article under the terms of the [Creative Commons Attribution-NonCommercial License](https://creativecommons.org/licenses/by-nc/4.0/), which permits use, distribution and reproduction in any medium, provided the original work is properly cited and is not used for commercial purposes.

Project Administration: Maria Tzortziou
Supervision: Maria Tzortziou
Validation: Alana Menendez, Maria Tzortziou, Patrick Neale, Patrick Megonigal, Philippe Schmitt-Kopplin, Michael Gonsior
Writing – original draft: Alana Menendez, Maria Tzortziou
Writing – review & editing: Patrick Neale, Patrick Megonigal, Leanne Powers, Michael Gonsior

transformations simultaneously occur (Bauer et al., 2013; Tzortziou et al., 2008, 2015; Ward et al., 2017). Terrestrial export of organic carbon from rivers and coastal wetlands supports estuarine heterotrophy (Raymond & Bauer, 2001), representing a significant source of CO₂ to the atmosphere (Borges et al., 2005). Based on national wetland inventories, the North American wetland carbon pool is 220 Pg, 98% of which is in the soil, with estuarine wetlands sequestering ~10-times more carbon per area than other wetland systems (Bridgman et al., 2006). While the effects of salt marsh productivity on adjacent water bodies—the Outwelling Hypothesis—has been demonstrated (Nixon, 1980), large uncertainties remain in quantifying this impact (Childers et al., 2002; Santos et al., 2021; Tobias & Neubauer, 2009). Knowledge on the magnitude of lateral advective exchange of carbon across the marsh-estuary interface is critical for understanding the role of marshes in coastal biogeochemistry and carbon budgets (Tzortziou et al., 2008, 2011).

In a compilation of salt marsh studies, 11-of-13 systems were found to export dissolved organic carbon (DOC) from marsh to estuary, however the amount of this export was variable, ranging from 15 to 328 g C m⁻² yr⁻¹ (Childers et al., 2002). Variability from site-to-site can be a result of differences in tidal range and inundation, geomorphology, age of the marsh, below and above ground biomass, or groundwater input (Childers et al., 2002). A challenge in synthesizing flux rates across studies is a lack of carbon mass attributed to a defined wetland area, which can be difficult due to complicated surface and subsurface hydrologic flows. With more lateral flux estimates being reported, we can better constrain the dominant physical and biogeochemical controls on these fluxes and create more accurate coastal carbon budgets. Najjar et al. (2018) suggests that there could be large uncertainties in net lateral carbon fluxes because of temporal variability, such as episodic events not captured during the period of flux calculation. This has been addressed in Saraceno et al. (2009), while Majidzadeh et al. (2017), Osburn et al. (2019), and Cao and Tzortziou (2021), examined the effects of hurricanes on increased DOC transport from wetlands to estuarine and coastal waters in the Eastern and Southeastern, USA, using field and satellite observations. Hurricane-like events are projected to increase in frequency and intensity along the U.S. Atlantic Coast (Bender et al., 2010), making the incorporation of these events into lateral flux budgets important for ensuring accurate coastal carbon budgets in the future.

Colored dissolved organic matter (CDOM) is the light absorbing and fluorescing pool of dissolved organic matter (DOM), defined in this study as filtrate passing through a 0.2 μm membrane filter. CDOM has high absorption in the ultraviolet (UV) and visible light wavelengths and therefore affects water column light attenuation, with implications for estuarine biogeochemical cycling, ecology, and ocean color (Bricaud et al., 1981). Analysis of CDOM optical properties can reveal information about DOM molecular structure, which alludes to DOM source, as well as fate once exported from the marsh into estuary (i.e., degradation pathways) (Boyd & Osburn, 2004; Fellman et al., 2010; Helms et al., 2008; Romera-Castillo et al., 2011; Stedmon et al., 2000; Tzortziou et al., 2008, 2011; Vodacek et al., 1997; Wagner et al., 2015). Due to its strong impact on ocean color, CDOM and, as a proxy, DOC concentrations can be estimated remotely from sensors at spatial scales ranging from ground-based to satellite, using water-leaving radiance, which allows for organic matter dynamics to be analyzed across systems (Cao et al., 2018; Cao & Miller, 2015; Mannino et al., 2008; Swan et al., 2013). Fluorescent dissolved organic matter (FDOM) can be measured in situ with optical sensors, is dependent on CDOM absorption ($a_{\text{CDOM}}(\lambda)$), and correlates strongly with DOC concentration ([DOC]) (Belzile et al., 2006; Tzortziou et al., 2011) in terrestrially-influenced aquatic environments. This uniquely enables FDOM sensors to be valuable tools for improving temporal understanding of CDOM and DOC dynamics in coastal waters, as quick and reliable FDOM measurements can allow for expanded datasets of these biogeochemical variables.

Building on previous work on lateral fluxes and transformations of DOC and CDOM in Chesapeake Bay tidal wetland-estuarine systems (Cao et al., 2018; Jordan & Correll, 1991; Logozzo et al., 2021; Tzortziou et al., 2008, 2011), this study applies high frequency observations to assess: (a) the use of water optical and other physicochemical properties measured in situ to retrieve [DOC] at a marsh-estuary interface; (b) temporal dynamics of marsh-estuary DOC exchange across a range of scales from diurnal to seasonal and inter-annual, and in response to both natural cycles as well as episodic events; and (c) the ability to link improved estimates of DOC flux with high resolution data on DOM quality, to better determine the sources and fate of marsh-exported organic matter and its potential impacts on coastal carbon budgets.

While this study focuses on a well-characterized tidal marsh ecosystem in the Chesapeake Bay, techniques and characterizations developed here can be used to scale-up to other temperate, brackish, tidal marshes. A robust temporal understanding of the carbon fluxes and transformations occurring at the marsh-estuary interface will

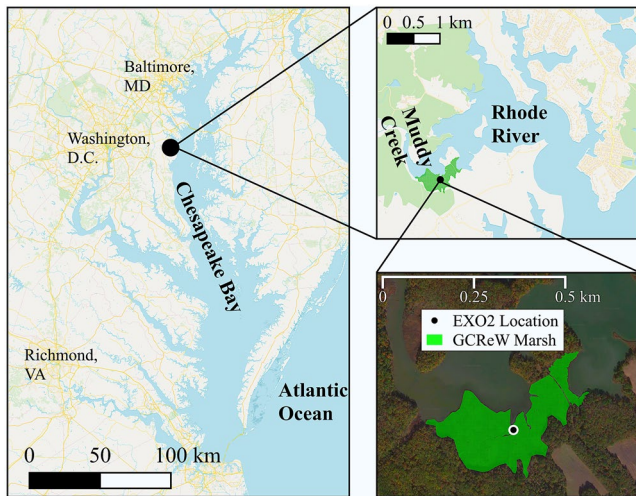


Figure 1. Maps of study area. The GCRew Marsh is located within the Rhode River sub-estuary along the northwestern shore of the Chesapeake Bay. The Muddy Creek is located northwest of the GCRew Marsh.

allow for improvements in coastal carbon cycle modeling by pinpointing typical flux concentrations from these productive ecosystems, as well as identifying larger fluxes that could be expected in more extreme instances. This work could also advance coastal DOC remote sensing satellite retrievals by increasing datasets needed for validation and ground truthing, as accurately estimating [DOC] based on in situ measurements can be done at scale.

2. Methods

2.1. Field Measurements

Kirkpatrick Marsh is a 22-ha brackish, high marsh located within the Rhode River, a shallow sub-estuary of the northwestern Chesapeake Bay, in Edgewater, Maryland (38.8741°N, 76.5481°W). The Global Change Research Wetland (GCRew) is a research facility on Kirkpatrick Marsh that supports long-term coastal wetland studies. GCRew is microtidal with a 0.44 m tidal range and plant communities dominated by *Spartina patens*, *Distichlis spicata*, *Schoenoplectus americanus*, *Iva frutescens* and *Phragmites australis* as determined by their mean elevation (Holmquist et al., 2021). Net ecosystem exchange (NEE) calculated over a 19-year study for GCRew was found to be between +1.5 and +1.9 kg C m⁻² yr⁻¹ (Erickson et al., 2013). Soils in the marsh platform are 80% organic matter to a depth of 5.5 m with somewhat higher mineral content within 10 m of the marsh-estuary interface.

Continuous monitoring was conducted at the GCRew marsh-estuary interface (Figure 1) tidal creek from fall 2014 to summer 2018. The GCRew tidal creek (Figure 1) is a conduit for semi-diurnal tidal waters draining 0.03 km² marsh area (Jordan & Correll, 1991). An EXO2 multiparameter sonde (YSI Inc.) was used to collect measurements every 15 min with probes 0.25 m from channel bottom. The EXO2 measures FDOM (excitation 365 ± 5 nm and emission 480 ± 40 nm), chlorophyll-*a* fluorescence (FChl-*a*) (excitation 470 ± 15 nm and emission 685 ± 20 nm), turbidity (excitation 860 ± 15 nm and measures scattering at 90° of the incident beam), pH, dissolved oxygen, temperature/conductivity, and water depth, allowing for a suite of water quality parameters to be known simultaneously during deployment. Calibrations were conducted pre and post instrument deployment probe-by-probe, using the protocols and calibration standards outlined in the YSI EXO2 manual. In particular, the FDOM sensor was calibrated to read 300 QSU for a 300 µg L⁻¹ quinine sulfate solution in 0.1 N H₂SO₄ at 22°C. The instrument was removed periodically for calibration, maintenance, and repair, and during freezing conditions. During most periods of EXO2 deployment within the GCRew tidal creek, a Sontek-IQ acoustic doppler velocimetry probe was also deployed at the channel bottom (sitting 5 cm above channel bed), mid-point of the creek width, ~1-m from the EXO2. The Sontek recorded water column velocity using four acoustic transducers, and water stage using a pressure transducer, at 5 or 15-min increments, based on averages over a 2-min time interval. Water flow was then calculated based on these measurements along with user-defined channel geometry (channel width = 1.85 m). Under our schematic, positive water flow values equated to the flood phase of the tidal cycle, with water entering the GCRew tidal creek flume, and negative values were associated with ebb tidal phases, where water exited the tidal creek into the Rhode River sub-estuary. To reduce effects of biofouling on instruments during deployments, the EXO2 contained a central wiper that cleaned probe surfaces and the Sontek periodically had its transducers scrubbed.

About once-a-month, from the fall of 2014 through 2016, a Teledyne ISCO-3700 series automatic water sampler was deployed for 24-hr periods, collecting hourly water samples over two semi-diurnal tidal cycles within the GCRew tidal creek. Water samples were filtered within 12 hr for optical analysis of CDOM and [DOC]. A Whatman GF/F glass microfiber 0.7 µm filter was used for pre-filtration, followed by a Whatman Nuclepore polycarbonate 0.2 µm filter, as outlined in the protocol of Cao et al. (2018). Filtered water was put in acid-washed, pre-combusted glass amber bottles and stored in the dark at 4°C for less than 1 week before optical analysis. CDOM absorbance measurements were run in duplicates on a CARY-IV dual-beam spectrophotometer, using acid-washed, 1-cm path-length quartz cuvettes and were baseline-corrected using DI water following the methodology in Tzortziou et al. (2011). CDOM absorbance was converted to absorption based on the Beer-Lambert law using

$$a_{\text{CDOM}}(\lambda) = 2.303A(\lambda)/l \quad (1)$$

where $a_{\text{CDOM}}(\lambda)$ is the absorption of CDOM at wavelength λ (nm), A is absorbance of CDOM at that wavelength, and l is the pathlength in m, here 0.01. Spectral slope of a_{CDOM} (S) was calculated in the spectral ranges of 275–295 nm ($S_{275-295}$) by fitting

$$a_{\text{CDOM}}(\lambda) = a_{\text{CDOM}}(\lambda_{\text{ref}})e^{-S(\lambda-\lambda_{\text{ref}})} \quad (2)$$

with λ_{ref} representing a reference wavelength and S is the spectral slope (nm^{-1}) (Green & Blough, 1994; Helms et al., 2008).

Refrigerated DOC samples were run in duplicates on a Shimadzu TOC-V CSH Total Organic Carbon Analyzer within 1-month of filtering following methods in Tzortziou et al. (2011).

For the monthly ISCO water sampling occurring in August 2015, August 2016, and October 2016, water samples were also collected for solid-phase extraction (SPE) (Dittmar et al., 2008) and analyzed by Fourier transform ion cyclotron resonance mass spectrometry (FT-ICR MS) (see Section 3.6).

Precipitation and wind data were obtained from the Smithsonian Environmental Research Center (SERC) meteorological tower (38.89°N, 76.56°W) in Edgewater, Maryland. Rainfall data at the tower was measured every minute using a TE525 tipping bucket gauge with 0.01-inch resolution. Wind speed and wind direction were measured using a R. M. Young 05103 Wind Monitor. Both rainfall and wind data were recorded with a CSI CR10X logger.

2.2. Application of FDOM Corrections

Data from the EXO2 FDOM sensor must be corrected for temperature and attenuation by particulate and dissolved materials (Downing et al., 2012). At higher water temperatures, a reduced fluorescence emission signal can be expected: the impact for humic-like organic matter has been found to be approximately a 1% decrease in fluorescence emission per degree C temperature increase (Henderson et al., 2009). Thus, a correction was applied using Equation 3, for a reference temperature of 25°C following Downing et al. (2012):

$$\text{FDOM}_{\text{corr_temp}} = \text{FDOM}_{\text{raw}} * (1 + 0.01 * [\text{Temp} - 25]) \quad (3)$$

where $\text{FDOM}_{\text{corr_temp}}$ is temperature corrected FDOM in quinine sulfate units (QSU), FDOM_{raw} is raw FDOM from the EXO2 in QSU, Temp is tidal creek water temperature (°C), and 0.01 corresponds to the 1% temperature coefficient (ρ in Watras et al., 2011) at 25°C determined empirically in the lab for the EXO2.

Attenuation of FDOM fluorescence in situ is a result of signal loss due to CDOM absorption as well as particulate absorption and scattering of light in both the excitation (from sensor to sample) and emission (from sample back to detector) directions. Corrections for attenuation were applied following temperature corrections (Equation 3), using the instrument specific (EXO2) correction function equations discussed in Snyder et al. (2018).

$$\text{FDOM}_{\text{intermediate}} = \frac{\text{FDOM}_{\text{corr_temp}}}{2.7183^{(-0.006 * \text{Turb})}} \quad (4)$$

$$\text{FDOM}_{\text{corr}} = (0.0044 * \text{FDOM}_{\text{intermediate}}^2) + (0.7324 * \text{FDOM}_{\text{intermediate}}) \quad (5)$$

This is a two-stage correction in which a non-linear correction for particulate components is first applied to $\text{FDOM}_{\text{corr_temp}}$ in QSU in Equation 4, where 2.7183 and -0.006 are coefficients for turbidity correction, and Turb is the EXO2 measured turbidity in formazin nephelometric units (FNU). High outliers for turbidity, attributed mostly to debris passing over the sensor, were removed using the Matlab Hampel function. The result of Equation 4 ($\text{FDOM}_{\text{intermediate}}$) is then used as a proxy for CDOM to further adjust for dissolved absorption using Equation 5, resulting in a fully corrected FDOM value ($\text{FDOM}_{\text{corr}}$). Downing et al. (2012) suggested that sensor corrections for attenuation be site-specific, given that particle size, shape, and material can vary. Yet, Saraceno et al. (2017) found that their site-specific corrections for FDOM attenuation were indistinguishable from the Downing et al. (2012) FDOM corrections up to 300 FNU, well above the turbidity range observed at GCReW.

2.3. DOC Measurements and Estimates of Water and DOC Fluxes

As part of our quality control protocol for DOC measurements, samples were flagged for >10% half-difference between duplicate measurements. Strong positive correlations have been shown between [DOC] and a_{CDOM} across a wide range of systems (Fichot & Benner, 2011; Mannino et al., 2008; Spencer et al., 2012), however, this relationship is seasonally and regionally dependent due to changes in the quality of DOC (Del Vecchio & Blough, 2004; Tzortziou et al., 2008, 2011). In our dataset, we observed seasonal and tidal variability in the DOC- $a_{\text{CDOM}}(300 \text{ nm})$ relationship and DOC values that proved to be outliers beyond the observed seasonal and/or tidal variability were flagged.

The DOC dataset, with flagged samples removed, was used to determine the relationship between [DOC] and the EXO2 variables: FDOM_{corr}, FChl-*a*, turbidity, pH, dissolved oxygen, salinity, and temperature. Overall, there were 256 DOC samples used that had concurrent EXO2 in situ measurements at the time of water sample collection. Multiple linear regression models were initially evaluated in Matlab with standardized EXO2 parameters (mean subtracted and divided by standard deviation) as the predictor variables and standardized [DOC] as the response variable. The choice of multiple linear regression model was based on the coefficient of determination as a goodness of fit and the statistical significance of the chosen predictor variables ($p < 0.05$). Multicollinearity was evaluated for the explanatory variables to ensure independence and the appropriateness of multiple linear regression application. Variance Inflation Factor (VIF) was calculated in Matlab for each of the explanatory variables.

The multiple linear regression model linking EXO2-measured water quality parameters to [DOC] was used to then estimate [DOC] for the full period of EXO2 deployment at the GCRew tidal creek (fall 2014 to summer 2018). At times of slight instrument offset (between the EXO2 and Sontek), on the scale of just minutes, the EXO2 variables were interpolated to match flowmeter sampling times. Moving 45-min means were calculated for the estimated and interpolated DOC and water flow datasets, using three data points when data was recorded in 15-min sampling intervals and nine data points when data was recorded in 5-min sampling intervals. DOC flux (in g per sampling interval) was then calculated by multiplying estimated [DOC] (g m^{-3}) moving means by water flow ($\text{m}^3 \text{ s}^{-1}$) moving means and integrating over defined time intervals.

Monthly DOC fluxes (kg C mon^{-1}) were estimated for months that had at least 14 full days of DOC flux data; this threshold was chosen to avoid bias toward spring or neap tides within a lunar cycle and resulted in 21 monthly estimates of DOC fluxes. To achieve this, average daily DOC flux within a given month was estimated based on observations and scaled up to a monthly DOC flux using number of days per month. To estimate DOC flux per tidal cycle and water flux per tidal cycle, we first identified gaps in existing datasets, and then integrated flux over consecutive, continuous 12.5-hr time intervals (reflective of semi-diurnal tides). For each of these tidal cycles ($n = 1,128$), low and high tide [DOC] (and similarly for tidal stage comparisons of EXO2 parameters) was estimated by averaging values ± 30 min around the time of minimum water depth for low tide and maximum water depth for high tide, identified using the Sontek flowmeter depth data. While tidal cycles were defined based on set 12.5-hr time intervals, flood tide and ebb tide water flow phases were demarked based on the periods from low tide depth to high tide depth, and high tide depth to low tide depth, respectively.

2.4. Error Estimates in DOC Fluxes

An average error of $\pm 13\%$ was found in estimating [DOC] based on the root mean squared error of the multilinear regression. An error of $\pm 1\%$ was applied to Sontek water flow data based on reported accuracy in instrument measured water velocity. Combined, this results in an estimated error of +14.13% and -13.87% in predicting DOC flux. This methodology reflects a one-sigma uncertainty and does not account for potential errors in EXO2 measurements of the explanatory variables used in creating the relationship to [DOC], or potential differences in water flow velocity across the tidal creek channel horizontally or vertically. This also does not consider potential errors in temporal extrapolations that were made in estimating monthly flux values and annual flux values for periods when instruments were not deployed within the GCRew tidal creek. Another possible source of error that is unaccounted for is the drainage area of the tidal creek, which was based on a literature value from 1991 and could have changed with altered wetland morphology since that time; this drainage area was used to calculate DOC flux per unit area of marsh.

2.5. Qualitative Assessment of DOM Composition Using Ultrahigh Resolution Fourier Transform Ion Cyclotron Resonance Mass Spectrometry (FT-ICR MS)

The ISCO sampler collected one 800 mL water sample per hour over a 24-hr period in August 2015, August 2016, and October 2016, for a total of 24 single samples per sampling event to capture two semi-diurnal tidal cycles. Again, within 12 hr of the final sample collection, samples were filtered through pre-combusted Whatman GF/F filters and extracted using 1 g/6 mL Agilent PPL solid phase extraction (SPE) cartridges. Briefly, samples were acidified to pH 2 using high purity HCl (puriss. p.a., $\geq 32\%$, Sigma Aldrich) and then gravity-fed at a flow rate of approximately 10 mL min^{-1} to the previously activated PPL cartridge. Activation of the PPL resin was achieved by using 5 mL methanol (LC-MS Sigma-Aldrich Chromasolv) followed by 10 mL 0.1% formic acid (LC-MS Sigma-Aldrich Chromasolv). After the sample had passed through the cartridge, it was rinsed with ultrapure water (18 M Ω MilliQ water, Barnstead) to remove salts and washed with 10 mL 0.1% formic acid to replace remaining salts and sample. After drying the cartridge under nitrogen, the cartridge was eluted with 10 mL methanol into pre-combusted amber glass vials. The methanolic extract was stored at -18°C , which is recommended for prolonged storage to preserve DOM in methanolic extracts (Flerus et al., 2011), prior to FT-ICR MS analysis in July 2017.

FT-ICR MS analysis were carried out at Helmholtz Zentrum München, Germany, using a 12 T Bruker Solarix FT-ICR MS. Each methanolic extract was diluted 1:40 and directly injected into the MS at a flow rate of $3 \mu\text{L min}^{-1}$. Five hundred scans at 4 mega words were collected and averaged to yield highly precise MS spectra with less than 0.2 ppm mass error. Mass lists were generated and exported using a signal-to-noise ratio cutoff ≥ 10 , which were subsequently aligned within an m/z window of 0.5 ppm using proprietary Matrix Generator software (Lucio, 2009). Exact and unambiguous formula assignments were based on the following atomic ranges: $\text{C}_{1-\infty}\text{H}_{1-\infty}\text{N}_{1-3}\text{O}_{1-30}\text{S}_{1-3}$. Formula assignments were achieved using a proprietary in-house algorithm that has been extensively used to accurately assign formulas (Powers et al., 2019, 2021; Valle et al., 2020). Exact molecular formula assignments were only considered valid if they met criteria outlined previously (Herzsprung et al., 2014; Koch et al., 2007). The data processing to evaluate the differences between tidal outflow and inflow was solely based on CHO signatures, because of the established van Krevelen space (van Krevelen, 1950) of presumed polyphenolic signatures that correlate well with terrestrially-derived CDOM (Gonsior et al., 2016; Powers et al., 2021) to characterize the outflow and much more pronounced aliphatic CHO signatures in the inflow.

3. Results

3.1. Seasonal and Tidal Patterns in Tidal Marsh Creek Physicochemical Properties

Seasonality strongly regulated physicochemical and biogeochemical conditions in the GCRew tidal creek (Figure 2; Table 1). $\text{FDOM}_{\text{corr}}$ was highest in summers, with values reaching 600 QSU (Figure 2b) and maxima in monthly median values either in July or August (from ~ 93 to ~ 153 QSU). $\text{FDOM}_{\text{corr}}$ was a factor of four, or more, lower in winter, with minimum monthly median values either in December or January ranging from ~ 21 QSU to 24 QSU. Highest dissolved oxygen (DO) was typically observed in January ($\sim 7 \text{ mg L}^{-1}$; Table 1), except in 2018 when the highest DO on record (monthly median of 10.58 mg L^{-1}) was measured in March. Lower DO medians were measured, as expected, during summer months (Figure 2d), with concentrations in July and August often $< 2 \text{ mg L}^{-1}$, representative of hypoxic conditions. Tidal Creek pH values were variable, ranging from 6.2 to 9.7 (Figure 2e), with high pH in spring months most likely corresponding to spring algal blooms and high sub-estuary primary productivity (Figure 2e and Table 1). Salinity ranged from ~ 1 to 16 PSU, with higher values typically in the fall and lower in winter and spring (Figure 2f; Table 1). Maxima in chlorophyll fluorescence, FChl-*a*, in April and May (~ 21 – $55 \mu\text{g L}^{-1}$, Table 1) were consistent with the occurrence of spring algal blooms, while minimum values were measured in late fall and winter (note: this is based on raw FChl-*a* data from the EXO2, which is calibrated using rhodamine WT dye). Seasonal cycles in turbidity were less clear, with the highest monthly median (~ 28 FNU) observed in March 2017, almost twice that of the second monthly maximum on record in January 2015 (Table 1).

Superimposed on seasonal cycles, semidiurnal tides were the dominant factor affecting variability at shorter timescales, particularly for $\text{FDOM}_{\text{corr}}$, DO, and pH (Figures 3b, 3d and 3e, Table 2). Monthly medians in low tide $\text{FDOM}_{\text{corr}}$ ranged from approximately 2-to-5 times higher than high tide $\text{FDOM}_{\text{corr}}$ (Table 2). Although seasonality in water quality parameters was observed independently of tidal influence, seasonality in $\text{FDOM}_{\text{corr}}$

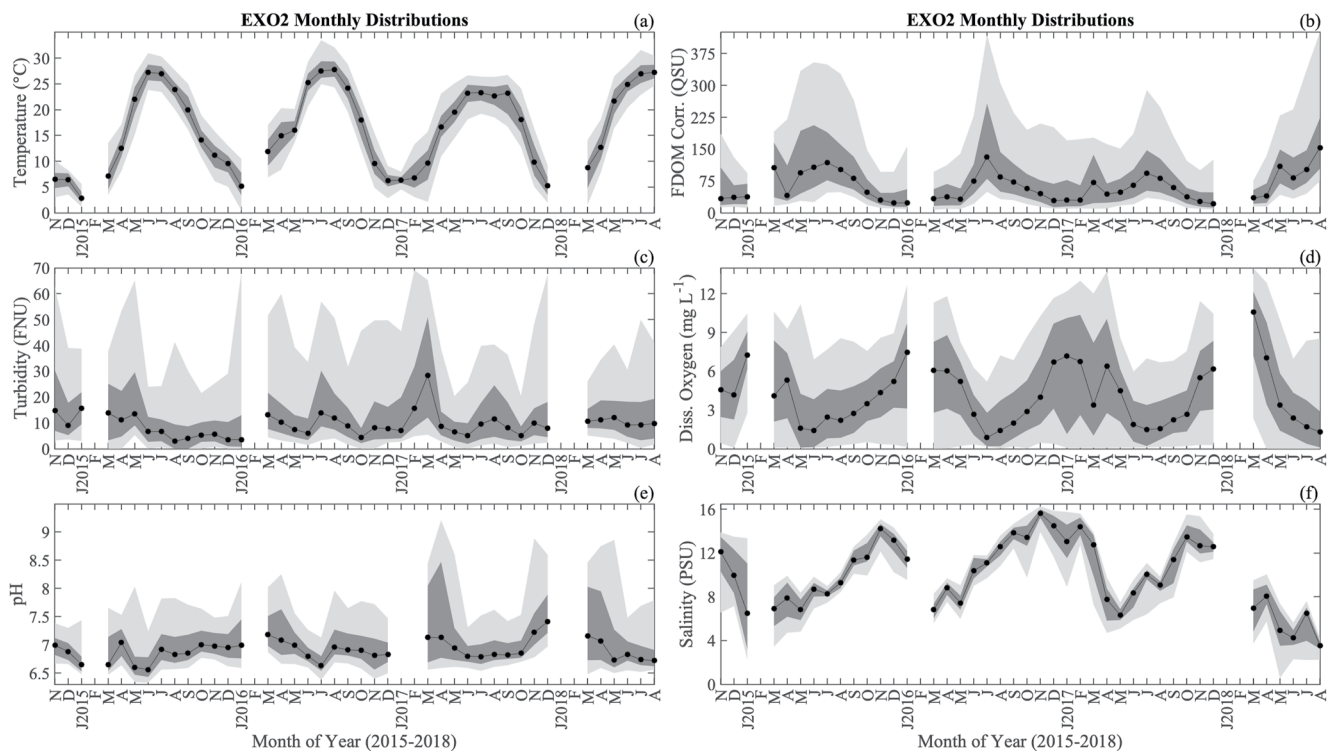


Figure 2. Monthly distributions in temperature (a) and the five EXO2 explanatory variables used for [DOC] prediction (FDOM_{corr} (b), turbidity (c), dissolved oxygen (d), pH (e), and salinity (f)). Monthly medians are shown with black dots, 25th to 75th percentiles of instantaneous values are in dark gray, and 5th to 95th percentiles of instantaneous values are in light gray. All deployment data from a given month, taken at 5 or 15-min sampling intervals, is shown here, thereby including all tidal phases and any potential episodic events.

was particularly pronounced at low tide (Figure 3b), when marsh export is the dominant source of DOM in this system. Low tide FDOM_{corr} values ranged from ~7 QSU in December-January to ~546 QSU in July and was >100 QSU in ~46% of the measurements ($n = 1,128$). FDOM_{corr} at high tide varied from ~5 to ~351 QSU, but with ~93% of measurements <100 QSU ($n = 1,128$) (Figure 3b). Compared to high tide, DO monthly median at low tide was ~1.8 times lower in winter and ~27 times lower in summer (Table 2). Using 2 mg O₂ L⁻¹ and 0.2 mg O₂ L⁻¹ as thresholds of hypoxia and anoxia, respectively (Hagy et al., 2004), ~60% of creek low tide values were hypoxic and ~18% were anoxic ($n = 1,128$), while only ~8% of creek high tide values were hypoxic and ~2% were anoxic ($n = 1,128$). Monthly median pH values were consistently higher at high tide, by ~5–28%, with highest values in April (Table 2). To a less clear extent, tidal cycles did play a role in tidal creek salinity. By examining differences between high tide and low tide salinity, ~11% of cycles had low tide water with salinity 0.5 PSU or greater than high tide water and ~29% of cycles had low tide water fresher than high tide by 0.5 PSU or greater, although most tidal cycles (~60%) did not see a salinity change between tidal stages greater than 0.5 PSU ($n = 1,128$). There was not a clear seasonal trend in these tidal cycle salinity changes.

3.2. Estimates of DOC Concentrations

Although [DOC] was strongly correlated with FDOM_{corr} ($R^2 = 0.6$), inclusion of additional EXO2 water quality parameters in a multiple regression model improved [DOC] prediction ($R^2 = 0.71$; Figure 4). The strongest combination of EXO2 explanatory variables for [DOC] prediction was: FDOM_{corr}, turbidity (Turb), dissolved oxygen (DO), pH, and salinity (Sal). These results are based on 256 observations, and all variables were found to be statistically significant with p-values of 9.58×10^{-33} (FDOM_{corr}), 1.36×10^{-10} (Turb), 1.05×10^{-8} (DO), 0.00891 (pH), and 0.0464 (Sal). Coefficients based on standardized variables in the linear regression model are 0.749 (FDOM_{corr}), -0.266 (Turb), -0.382 (DO), 0.152 (pH), and -0.0789 (Sal). Based on this model,

$$[\text{DOC}]_{\text{est}} = (0.022 * \text{FDOM}_{\text{corr}}) + (-0.053 * \text{Turb}) + (-0.273 * \text{DO}) + (0.872 * \text{pH}) + (-0.071 * \text{Sal}) + 1.041 \quad (6)$$

Table 1
Monthly Medians From the EXO2 and Sontek Instruments Deployed Within the GCRW Tidal Creek, Along With Estimated [DOC] Based on Our Multilinear Regression Model

Month	FDOM (QSU)	Turb. (FNU)	Oxyg. (mg L ⁻¹)	pH	Sal. (PSU)	Temp. (°C)	FChl- <i>a</i> (µg L ⁻¹)	Est. DOC (g m ⁻³)	Flow (m ³ s ⁻¹)	Sontek depth (m)
Nov-2014	33.76	14.72	4.58	6.99	12.11	6.48	6.99	5.16	-	-
Dec-2014	36.06	8.97	4.17	6.88	9.96	6.43	2.26	5.28	-	-
Jan-2015	38.07	15.63	7.25	6.65	6.51	2.81	0.46	4.57	-	-
Feb-2015	-	-	-	-	-	-	-	-	-	-
Mar-2015	106.58	13.82	4.10	6.65	6.93	7.15	5.30	6.96	-	-
Apr-2015	40.95	11.10	5.31	7.04	7.88	12.49	5.31	5.58	-	-
May-2015	94.78	13.51	1.59	6.60	6.82	22.04	20.77	7.19	-	-
Jun-2015	107.05	6.66	1.42	6.56	8.68	27.23	7.73	7.62	-	-
Jul-2015	118.40	6.72	2.44	6.92	8.29	27.01	13.82	8.17	-	-
Aug-2015	102.31	2.94	2.20	6.83	9.28	23.91	16.09	7.87	-	-
Sep-2015	80.81	4.03	2.75	6.85	11.36	19.93	14.44	7.16	-0.0077	0.92
Oct-2015	47.95	5.26	3.49	7.00	11.63	14.11	11.05	6.16	-0.0220	0.83
Nov-2015	29.92	5.56	4.35	6.98	14.24	11.14	5.73	5.38	-0.0159	0.71
Dec-2015	23.20	3.47	5.21	6.95	13.18	9.52	7.30	5.09	-0.0241	0.72
Jan-2016	23.50	3.50	7.45	6.99	11.46	5.19	6.29	4.66	-0.0273	0.71
Feb-2016	-	-	-	-	-	-	-	-	-	-
Mar-2016	33.27	13.22	6.06	7.18	6.83	11.88	9.90	5.22	-0.0046	0.75
Apr-2016	37.83	10.33	6.03	7.08	8.81	14.91	21.61	5.20	-0.0146	0.81
May-2016	32.07	7.46	5.21	6.99	7.44	15.99	14.05	5.49	-	-
Jun-2016	74.80	6.06	2.66	6.80	10.39	25.24	8.44	6.75	-0.0278	0.81
Jul-2016	131.49	13.90	0.87	6.63	11.10	27.54	12.96	7.97	-0.0165	0.74
Aug-2016	84.26	11.87	1.43	6.96	12.58	27.75	18.61	7.52	-0.0250	0.80
Sep-2016	72.95	8.88	1.99	6.91	13.84	24.17	13.82	6.77	-0.0527	0.93
Oct-2016	57.12	4.43	2.89	6.90	13.45	17.96	9.12	6.30	-0.0236	0.85
Nov-2016	44.89	8.13	4.00	6.81	15.63	9.55	9.55	5.25	-0.0081	0.73
Dec-2016	28.58	7.82	6.70	6.83	14.51	6.23	10.28	4.90	-	-
Jan-2017	30.07	7.04	7.17	-	13.07	6.31	8.40	-	-	-
Feb-2017	29.47	15.62	6.76	-	14.41	6.74	13.02	-	-	-
Mar-2017	71.57	28.37	3.38	7.13	12.76	9.64	11.34	4.85	-0.0181	0.77
Apr-2017	44.19	8.63	6.40	7.13	7.76	16.66	55.42	5.83	-0.0159	0.81
May-2017	48.57	6.60	4.48	6.94	6.33	19.53	11.72	6.22	-0.0209	0.91
Jun-2017	65.21	5.14	1.87	6.80	8.35	23.24	11.94	7.05	-0.0177	0.88
Jul-2017	93.02	9.58	1.50	6.79	10.04	23.30	12.50	7.60	-0.0228	0.88
Aug-2017	81.53	11.63	1.55	6.83	9.08	22.68	10.89	7.36	-0.0405	0.94
Sep-2017	59.61	8.08	2.25	6.82	11.39	23.24	6.02	6.67	-0.0429	0.96
Oct-2017	37.51	5.12	2.66	6.85	13.47	18.10	5.28	5.90	-0.0240	0.87
Nov-2017	26.25	9.91	5.48	7.22	12.66	9.79	9.43	5.10	-0.0118	0.78
Dec-2017	20.99	7.93	6.19	7.41	12.59	5.29	5.73	5.02	-0.0041	0.69
Jan-2018	-	-	-	-	-	-	-	-	-	-
Feb-2018	-	-	-	-	-	-	-	-	-	-
Mar-2018	35.00	10.68	10.58	7.16	6.98	8.77	17.31	4.21	-	-

Table 1
Continued

Month	FDOM (QSU)	Turb. (FNU)	Oxyg. (mg L ⁻¹)	pH	Sal. (PSU)	Temp. (°C)	FChl- <i>a</i> (µg L ⁻¹)	Est. DOC (g m ⁻³)	Flow (m ³ s ⁻¹)	Sontek depth (m)
Apr-2018	40.08	11.21	7.03	7.07	8.06	12.72	20.60	5.18	-0.0118	0.76
May-2018	109.26	12.04	3.37	6.73	4.93	21.67	16.09	7.41	-0.0140	0.80
Jun-2018	82.69	9.20	2.38	6.83	4.24	24.90	13.49	7.36	-0.0407	0.96
Jul-2018	101.84	9.30	1.71	6.74	6.50	26.95	13.75	7.74	-0.0301	0.94
Aug-2018	153.53	9.72	1.29	6.72	3.53	27.26	15.31	9.34	-0.0283	0.90

In Equation (6), FDOM_{corr} (QSU), Turb (FNU), DO (mg L⁻¹), pH (unitless), and Sal (PSU) are all un-standardized variables from the EXO2, with VIF values less than 5 (3.20, 1.55, 4.15, 3.55, and 1.34, respectively), a threshold where multicollinearity between variables may be of concern.

Estimated [DOC] within the tidal creek ranged from 1.6 to 16.7 g m⁻³, with higher values consistently observed at low tide, especially during the summer months (Tables 1 and 2; Figure 5). Integrated across tidal stage, monthly medians in [DOC] showed minimum values (~4.5 g m⁻³) in winter or early spring and increased by almost a factor of two (~8 g m⁻³) in summer, with maxima typically observed in July (Table 1). This seasonal cycle in [DOC] was significantly more pronounced at low tide conditions (i.e., marsh export) than high tide (i.e., estuarine influence) (Figure 5). At low tide, monthly median [DOC] increased by about a factor of two from winter (~5 g m⁻³) to summer (~9–11 g m⁻³), while high tide [DOC] showed reduced seasonality changing from ~4 to 5 g m⁻³ in winter to ~6–8 g m⁻³ in summer.

3.3. GCRew Tidal Creek Water Flow

Ebb tides were found to have slightly faster average instantaneous water flows than flood tides (mean of -0.14 m³ s⁻¹ and median of -0.10 m³ s⁻¹ based on 1,009 ebb tides vs. 0.11 m³ s⁻¹ mean and 0.07 m³ s⁻¹ median based on 1,027 flood tides). Water fluxes were calculated for 1,128 tidal cycles based on data periods of 12.5 hr (Figure 6), and ~82% were within ±4,000 m³ tidal cycle⁻¹, while ~46% were within ±1,000 m³ tidal cycle⁻¹. Of these tidal cycles, 738, or ~65% resulted in a net export of water. The greatest water flux occurred on 1 October 2015, with ~22,609 m³ of water exported in a 12.5-hr period associated with Hurricane Joaquin (Figure 6; Figure 9a). The greatest import of water into GCRew occurred on 30 August 2017, with ~9,561 m³ of water entering during a tidal cycle. This tidal cycle, which began at the latter part of a flooding tide, underwent a large water depth change. Water depth was ~0.7 m at low tide prior to this captured cycle and had doubled to ~1.40 m at high tide (99th percentile for high tide depth; *n* = 1,127) following this cycle. During the tidal cycle, low tide depth was ~1.08 m, which is the 98th percentile for depth at low tide (*n* = 1,111).

Overall, net water flow volumes per tidal cycle, calculated as the average of flood and ebbing tide volumes, were consistent with GCRew high marsh values from Jordan and Correll (1991): their values ranged from ~0 to 5,600 m³ per tide, while we found a range of ~50–14,800 m³ per tide, with a tidal cycle mean of ~3,200 m³ (*n* = 996). Freshwater discharge was estimated based on a methodology of Jordan and Correll (1991), where it was assumed that ebb water volume equaled flood water volume plus freshwater discharge. Here it was found that ~68% of the ebb water volumes were greater than flood water volumes, resulting in a net “freshwater discharge,” while the remainder had flood volume exceeding ebb volume. The highest “freshwater discharge” (~21,087 m³) occurred on 1 October 2015, during Hurricane Joaquin, but out of the 673 tidal cycles with a “freshwater discharge” estimated, ~50% of these discharges were less than 1,000 m³ for the tidal cycle.

3.4. Marsh-DOC Lateral Export

Monthly mean DOC flux per tidal cycle during our record was consistently negative (Table 3), indicating consistent net export of DOC from the marsh to the estuary. Although FDOM_{corr} and [DOC] showed a clear seasonal cycle with higher monthly median values always during summer (Table 1), net marsh-DOC lateral export was higher typically in early fall (Table 3) driven by both variability in [DOC] and water fluxes. The highest DOC monthly fluxes occurred in September and October 2016, with a net export of ~1,218 kg C and ~988 kg C,

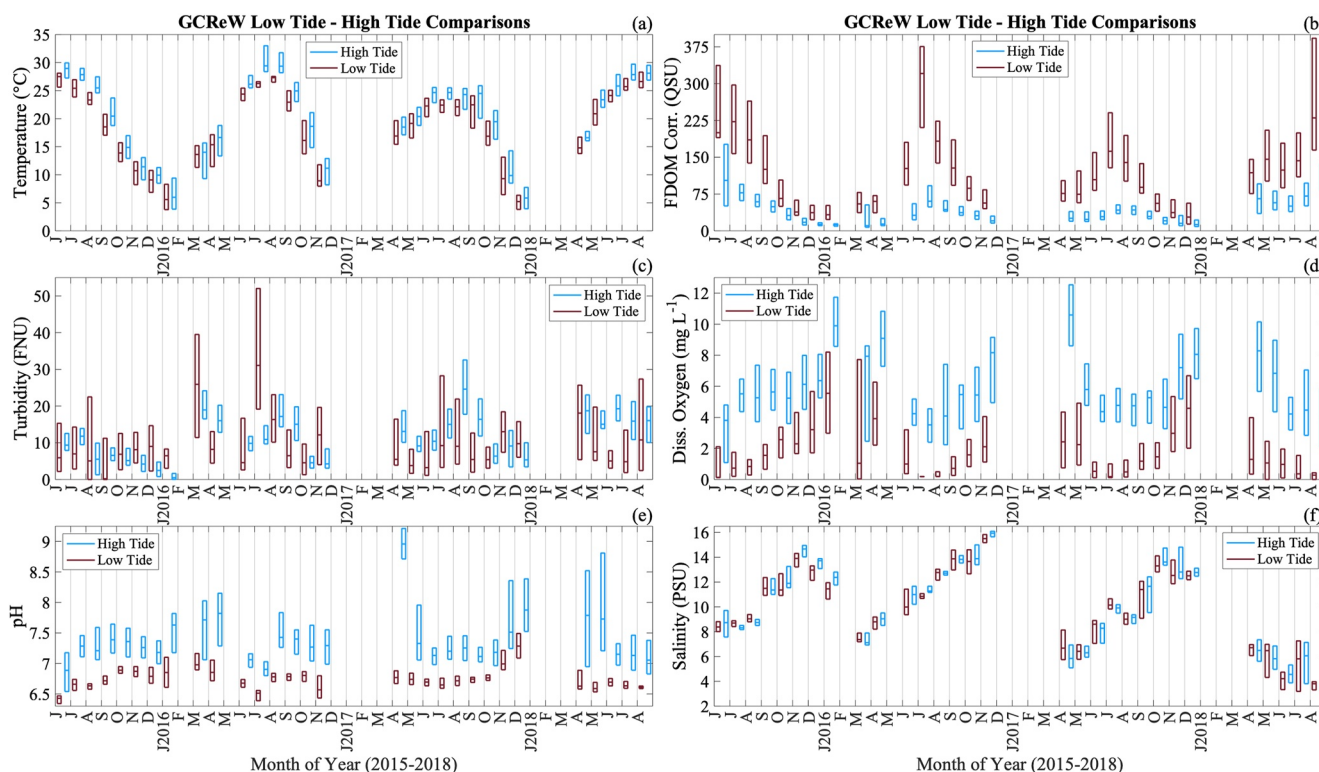


Figure 3. YSI EXO2 parameters from Figure 2: temperature (a), $FDOM_{corr}$ (b), turbidity (c), dissolved oxygen (d), pH (e), and salinity (f) separated into monthly box plots with low tide (maroon, to the left for each month) versus high tide (light blue, to the right for each month) phases within the GCRew tidal creek for June 2015 to August 2018. Median values are displayed with horizontal lines within the boxes, and the boxplots extend to 25th and 75th percentiles of all values.

respectively (Figure 7; Table 3). During these two months, monthly median [DOC] at low tide was $>7 \text{ g m}^{-3}$, while mean water flux per tidal cycle was among the highest on record ($-1,500 \text{ m}^3 \text{ cycle}^{-1}$ and $-2,042 \text{ m}^3 \text{ cycle}^{-1}$, respectively, Table 3). September 2016, with a total rainfall of $\sim 104 \text{ mm}$ at SERC (compared to a 2016 monthly average of $\sim 60 \text{ mm}$), was the second wettest month in 2016 after May (May 2016 did not have continuous in situ data for this study). On the contrary, while mean water flux per tidal cycle was among the highest on our record in December 2015 (Table 3), and there were enough tidal cycles measured to extrapolate a monthly DOC flux, DOC export was not particularly high, due to the significantly lower [DOC] at low tide in winter (Figure 7; Table 2). Indeed, the lowest DOC monthly flux, with a net export of $\sim 62 \text{ kg C}$ (Figure 7; Table 3), occurred in December 2017 when both monthly median [DOC] at low tide as well as water depth and water flux per tidal cycle were among the lowest observed (Tables 2 and 3). Water depth—a proxy for tidal marsh inundation—is an important control on tidal creek DOC flux intrinsically given the tidal nature of this system. September 2016 and September 2017, both corresponding to the annual peaks in DOC monthly fluxes to the estuary for these 2 years, had the highest median Sontek depth in each year (0.93 and 0.96 m, respectively) and among the highest monthly median instantaneous water flows ($\sim -0.05 \text{ m}^3 \text{ s}^{-1}$ and $\sim -0.04 \text{ m}^3 \text{ s}^{-1}$, respectively) on our record (Table 1).

Over our record, the average monthly DOC flux was $-530.77 \text{ kg C month}^{-1}$, which, when scaled up to an entire year and assuming the tidal creek drains a wetland area of 0.03 km^2 (Jordan & Correll, 1991), corresponds to an estimated export of $212.31 (+30.00/-29.45) \text{ g C m}^{-2} \text{ yr}^{-1}$. Here, we had DOC fluxes estimated for 1,128 tidal cycles based on in situ measurements of EXO2 explanatory variables and water flow (Figure 8). Of these 1,128 tidal cycles, 817 cycles (or, 72%) indicated a net export of DOC. Mean DOC flux from GCRew was $-8.59 (+1.21/-1.19) \text{ kg C a tidal cycle}$, and assuming 12.5-hr tidal cycles, there would be 700.8 tidal cycles each year, which would infer annual GCRew export of $200.66 (+28.35/-27.83) \text{ g C m}^{-2} \text{ yr}^{-1}$ according to mean flux per tidal cycle and wetland drainage area. The estimated annual flux for GCRew using the estimated monthly data (Figure 7) above falls close to the export estimated using mean flux per tidal cycle (Figure 8), revealing general consistency in retrieved GCRew fluxes under different methodologies for arriving at an annual flux.

Table 2

Monthly Medians of Low Tide (LT) Versus High Tide (HT) Conditions Within the GCRew Tidal Creek Based on the EXO2 Sonde

Month	DOC LT	DOC HT	FDOM LT	FDOM HT	Turb. LT	Turb. HT	Oxyg. LT	Oxyg. HT	pH LT	pH HT	Sal. LT	Sal. HT	Temp. LT	Temp. HT	Depth LT	Depth HT
Jun-2015	10.16	7.19	200.04	102.73	5.90	9.35	0.14	3.81	6.43	6.89	8.38	8.73	27.50	28.96	0.73	0.94
Jul-2015	10.57	6.30	222.43	77.48	6.98	11.78	0.73	5.51	6.66	7.29	8.70	8.32	25.43	27.86	0.78	1.07
Aug-2015	9.50	6.24	185.31	59.19	5.07	5.51	0.84	5.26	6.63	7.21	9.04	8.74	23.34	25.48	0.70	1.04
Sep-2015	8.38	5.78	126.83	49.24	0.19	6.78	1.55	5.64	6.72	7.39	11.49	11.43	18.45	20.29	0.78	1.06
Oct-2015	6.71	5.39	65.92	31.46	6.88	5.16	2.56	5.24	6.89	7.36	11.36	11.90	13.88	14.89	0.69	0.97
Nov-2015	5.85	4.84	38.31	17.46	8.13	4.21	2.30	6.13	6.87	7.26	13.91	14.66	10.73	11.41	0.53	0.85
Dec-2015	5.50	4.74	37.00	13.00	9.01	2.45	3.21	6.36	6.79	7.18	12.96	13.72	9.08	9.93	0.60	0.87
Jan-2016	5.02	4.31	32.70	12.62	6.46	0.49	5.55	9.90	6.85	7.63	11.45	12.38	5.58	5.99	0.62	0.88
Feb-2016	–	–	–	–	–	–	–	–	–	–	–	–	–	–	–	–
Mar-2016	6.00	4.48	54.84	9.15	25.92	18.58	1.05	7.81	6.98	7.73	7.36	7.06	13.62	14.00	0.59	0.93
Apr-2016	5.99	4.18	60.01	13.71	8.21	16.03	3.91	9.04	6.85	7.81	8.79	9.03	15.35	16.61	0.71	0.98
May-2016	–	–	–	–	–	–	–	–	–	–	–	–	–	–	–	–
Jun-2016	7.95	5.53	127.07	31.68	4.59	9.84	1.00	4.24	6.68	7.06	9.99	11.00	24.38	26.14	0.67	0.96
Jul-2016	10.48	6.01	320.56	60.35	31.08	10.90	0.19	3.52	6.51	6.90	10.84	11.28	26.27	29.42	0.55	0.87
Aug-2016	8.70	5.62	182.72	43.33	16.32	17.16	0.20	4.09	6.78	7.43	12.77	12.71	27.32	29.35	0.65	0.95
Sep-2016	8.27	5.08	128.00	36.78	6.48	15.03	0.71	5.38	6.78	7.39	13.87	13.89	22.94	24.89	0.78	1.07
Oct-2016	7.09	5.26	86.74	30.39	4.55	4.55	1.59	5.79	6.80	7.30	13.66	13.89	16.13	18.61	0.70	1.04
Nov-2016	5.78	4.18	56.71	20.36	12.15	4.34	2.11	8.16	6.57	7.29	15.50	15.90	8.91	11.17	0.60	0.89
Dec-2016	5.60	4.34	70.01	22.59	14.13	3.62	3.19	7.87	6.60	7.22	15.52	16.22	10.99	10.29	0.70	0.89
Jan-2017	–	–	–	–	–	–	–	–	–	–	–	–	–	–	–	–
Feb-2017	–	–	–	–	–	–	–	–	–	–	–	–	–	–	–	–
Mar-2017	–	–	–	–	–	–	–	–	–	–	–	–	–	–	–	–
Apr-2017	7.00	5.32	76.21	25.56	5.47	13.10	2.42	10.59	6.77	8.96	6.67	5.85	16.91	18.50	0.71	1.02
May-2017	7.21	5.59	74.50	23.38	3.81	9.14	2.25	5.79	6.74	7.33	6.42	6.30	19.16	20.39	0.77	1.06
Jun-2017	8.32	5.55	104.31	28.85	3.23	10.40	0.53	4.37	6.70	7.13	8.60	8.28	22.26	24.65	0.71	1.02
Jul-2017	8.85	5.47	162.15	42.51	9.23	15.20	0.19	4.82	6.65	7.21	10.15	9.91	22.42	24.67	0.70	1.05
Aug-2017	8.75	5.24	139.15	41.74	9.03	24.18	0.48	4.68	6.72	7.25	9.01	9.16	22.11	24.33	0.76	1.08
Sep-2017	7.49	4.86	88.69	29.41	5.44	16.96	1.18	5.25	6.74	7.11	11.40	11.72	22.48	24.34	0.81	1.10
Oct-2017	6.39	4.96	56.01	20.60	5.40	6.37	1.46	4.64	6.76	7.18	13.30	13.61	16.87	19.46	0.72	1.01
Nov-2017	5.48	4.91	37.13	14.95	13.02	8.85	2.98	7.26	6.99	7.52	12.53	12.82	9.30	9.81	0.65	0.90
Dec-2017	5.23	4.95	28.14	12.71	9.76	5.34	4.59	8.06	7.29	7.88	12.50	12.77	5.22	5.85	0.58	0.84
Jan-2018	–	–	–	–	–	–	–	–	–	–	–	–	–	–	–	–
Feb-2018	–	–	–	–	–	–	–	–	–	–	–	–	–	–	–	–
Mar-2018	–	–	–	–	–	–	–	–	–	–	–	–	–	–	–	–
Apr-2018	7.80	5.33	118.45	60.81	18.07	18.63	1.29	8.09	6.63	7.45	6.71	6.20	14.79	16.41	0.67	0.94
May-2018	8.50	6.27	145.87	57.49	7.54	15.00	1.06	7.03	6.59	7.77	6.47	5.83	20.89	23.49	0.66	0.96
Jun-2018	8.78	5.78	123.86	50.04	5.04	19.01	0.97	4.17	6.69	7.13	4.22	4.55	24.14	25.76	0.78	1.10
Jul-2018	9.17	6.05	142.80	68.73	4.83	16.13	0.36	4.58	6.63	7.15	5.81	6.02	25.71	28.01	0.76	1.07
Aug-2018	10.93	7.59	230.07	98.80	10.77	16.04	0.28	3.88	6.61	7.06	3.81	3.54	26.63	28.10	0.77	1.03

Note: Units are as follow: DOC (g m⁻³); FDOM (QSU); Turbidity (FNU); Dissolved Oxygen (mg L⁻¹); pH (unitless); Salinity (PSU); Temperature (°C); Depth (m).

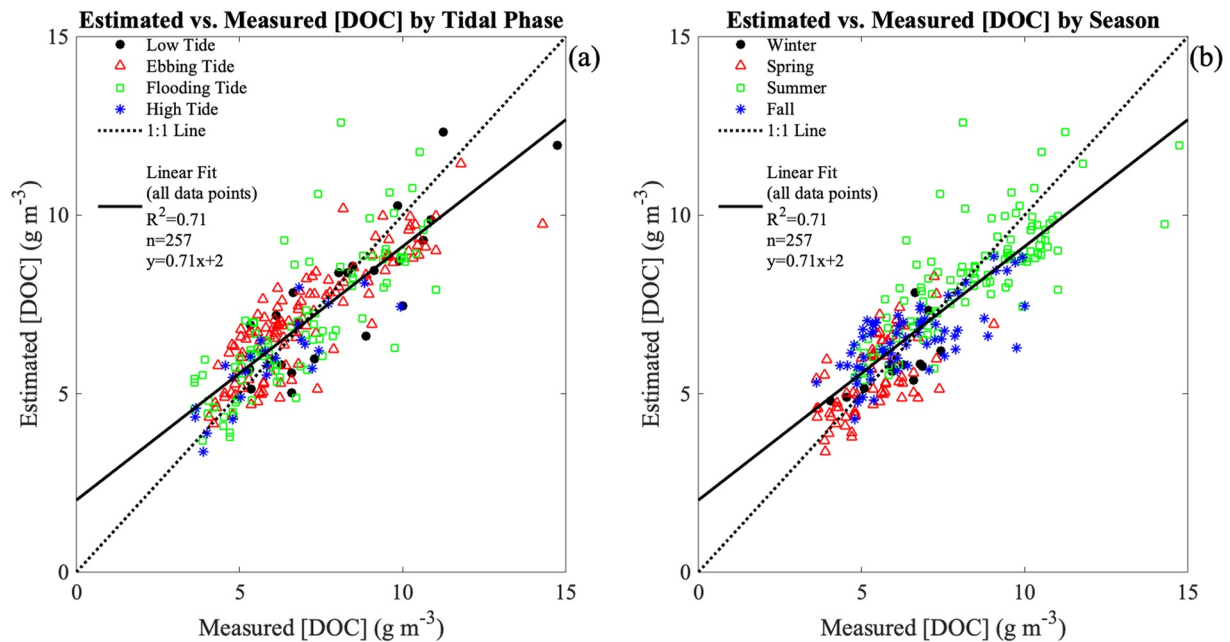


Figure 4. [DOC] estimated based on the explanatory variables of $FDOM_{corr}$, turbidity, dissolved oxygen, pH, and salinity is plotted versus measured [DOC] from water samples collected within the GCRew tidal creek from late 2014 through 2016, with samples representative of all tidal stages and seasons. Data points are coded by the tidal phase of collected sample in (a), and by season in (b).

3.5. Impact of Extreme Precipitation on Marsh DOC Flux

At the most extreme cases, water flow within the tidal creek draining GCRew ranged from approximately $-2 \text{ m}^3 \text{ s}^{-1}$ to $+2 \text{ m}^3 \text{ s}^{-1}$ (Figure 9a). The two most extreme DOC fluxes per tidal cycle recorded within this study period occurred on 1 October 2015 (Figure 9). On this date, consecutive tidal cycle fluxes were approximately -119 and -201 kg C (Figure 9b), which together would represent $\sim 5.32\%$ of the annual DOC flux calculated above based on the mean flux per tidal cycle. These high flux events align with precipitation and winds from Hurricane Joaquin, a Category 4 tropical cyclone. There was a total of $\sim 98 \text{ mm}$ of rain at the nearby SERC meteorological

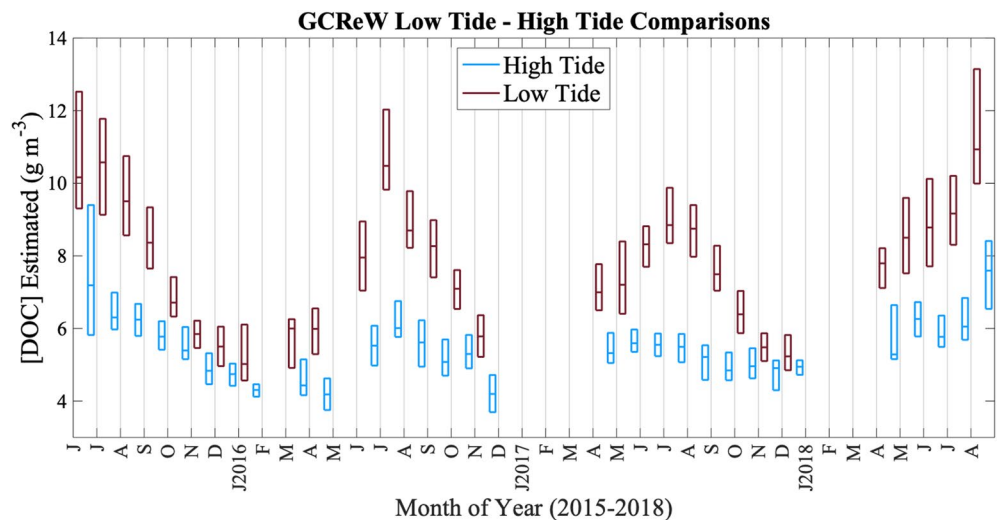


Figure 5. [DOC] estimated from the EXO2 explanatory variables of $FDOM_{corr}$, turbidity, dissolved oxygen, pH, and salinity is separated into boxplots associated with low tide (maroon, to the left for each month) versus high tide (light blue, to the right for each month) instances within the GCRew tidal creek for June 2015 to August 2018. The boxplots display medians, 25th and 75th percentiles.

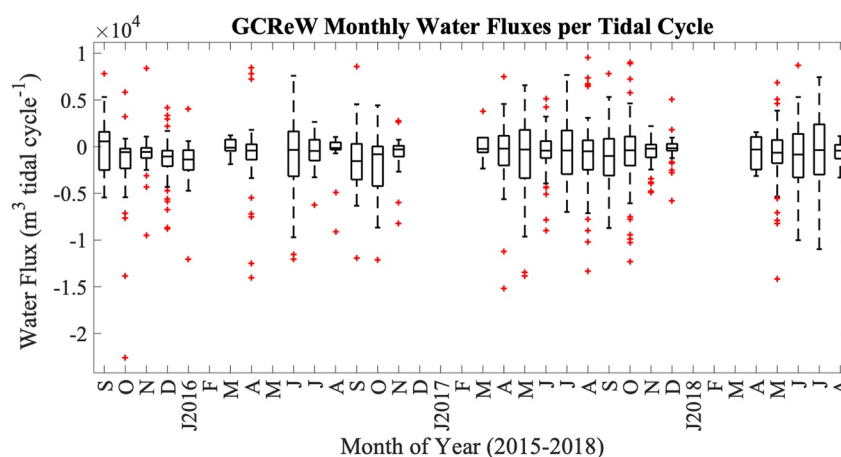


Figure 6. Net water fluxes, as measured by the Sontek, are shown from the GCRew tidal marsh for 1,128 tidal cycles. Positive values indicate water moving from the Rhode River sub-estuary into the wetland tidal creek, while negative values indicate water draining the tidal creek and moving toward the sub-estuary. The boxplots display medians, 25th and 75th percentiles, and whiskers extending to $\pm 2.7\sigma$, with outside that range considered outliers (shown with red +).

tower over the period of September 29 to 3 October 2015, with a total of ~ 55 mm just through October 1 (Figure 9c). With this onset of precipitation, there was an immediate freshening of the tidal creek by ~ 3 PSU. Wind direction was analyzed to decipher effects on water movement within the GCRew tidal creek flume for this storm event resulting in high DOC fluxes. On 29 September 2015, wind shifted from easterlies to southeasterlies. For the first half of September 30, winds were blowing from the southwest, but by the second half of the day, winds were coming from due north, which would facilitate water movement out of the tidal creek into Rhode River. This is shown by depressed water depth, where high tide water depth (0.76 m) is below bankfull depth on 1 October 2015 (Figure 9b). Over the next couple days as winds shifted from northerly to northeasterly to near-easterly, water depth rebounded. On the second half of October 2, freshwater inputs were observed (evident by a decrease in salinity during low tide) corresponding to some sustained rain (Figure 9c). There is a net water import during this tidal cycle, with a high low tide water depth (0.87 m) possibly due to the freshwater volume entering the creek, followed by a high, high tide (1.29 m) (Figure 9b).

3.6. Quality of Marsh-Exported DOC

DOC-specific CDOM absorption at 300 nm ($a_{\text{CDOM}}^*(300)$), calculated as the ratio between $a_{\text{CDOM}}(300)$ and [DOC], was overall significantly higher in water samples collected from this system at low tide compared to high tide. Based on GCRew tidal creek ISCO data using measured [DOC], in both 2015 and 2016, $a_{\text{CDOM}}^*(300)$ ranged from ~ 1.5 to $2 \text{ m}^2 \text{ g}^{-1}$, both from high tides in April, to ~ 5.5 – $6 \text{ m}^2 \text{ g}^{-1}$, both from low tides in July. This range indicates some of the variability in quality of DOM for this system across tides and seasons. August 2015, August 2016, and October 2016 samples all showed an increase in CDOM absorption, $a_{\text{CDOM}}(300)$, by more than a factor of two (Figure 10e), and considerably higher $a_{\text{CDOM}}^*(300)$ at low tide than high tide (Figure 10g). These results suggest that not only is GCRew a source of DOC to the adjoining Rhode River sub-estuary, but it is also a source of strongly colored and highly aromatic DOM in summer and fall, which has significant implications for estuarine photochemistry and biogeochemistry (Tzortziou et al., 2008). In addition, low tide DOM was consistently characterized by lower $S_{275-295}$ (Figure 10f), indicative of more aromatic, larger molecular weight material that has not yet undergone photobleaching (Helms et al., 2008; Logozzo et al., 2021).

FT-ICR MS showed consistent results with our optical analyses between low versus high tide data across the three comparisons in August 2015, August 2016, and October 2016 (Figures 10a–10c). In all 3 months, the low tide samples depict a lower H/C ratio centered around 0.8 and a higher O/C ratio centered around 0.6 than high tide samples. Higher H/C centered around 1.4 and lower O/C ratios centered around 0.4–0.5 in high tide samples correlated with higher chlorophyll concentrations (data not shown), and are indicative of aliphatic compounds and presumably autochthonous (e.g., algal derived) DOM (Powers et al., 2021).

Table 3
Monthly Means Are Shown for Fluxes of Water and DOC Per Tidal Cycle, Along With the Number of Tidal Cycles Represented by the Study in Each Month, and the Scaled-Up Estimates of Monthly DOC Flux, Which Were Calculated for Months With at Least 14+ Days of Data Represented

Month	Mean water flux per tide (m ³ cycle ⁻¹)	Mean DOC flux per tide (kg C cycle ⁻¹)	Number of tidal cycles analyzed	Est. Monthly flux (kg C month ⁻¹)
Sep-2015	33.68	-3.51	29	-215.80
Oct-2015	-1723.30	-13.88	53	-845.33
Nov-2015	-749.24	-4.60	47	-273.32
Dec-2015	-1458.50	-7.82	58	-474.20
Jan-2016	-1858.36	-8.69	20	-
Feb-2016	-	-	0	-
Mar-2016	-3.06	-1.13	14	-
Apr-2016	-865.64	-6.84	49	-385.60
May-2016	-	-	0	-
Jun-2016	-1299.24	-11.90	36	-676.28
Jul-2016	-714.15	-7.16	15	-
Aug-2016	-790.55	-11.25	16	-
Sep-2016	-1499.88	-18.62	45	-1226.45
Oct-2016	-2041.52	-17.58	46	-988.42
Nov-2016	-624.97	-4.83	55	-275.64
Dec-2016	-	-	0	-
Jan-2017	-	-	0	-
Feb-2017	-	-	0	-
Mar-2017	221.82	-0.69	6	-
Apr-2017	-528.28	-4.40	57	-248.51
May-2017	-865.57	-7.70	60	-441.71
Jun-2017	-600.36	-7.30	57	-433.05
Jul-2017	-534.76	-8.92	52	-561.39
Aug-2017	-789.42	-13.86	47	-806.16
Sep-2017	-1019.19	-14.19	42	-830.73
Oct-2017	-749.52	-7.80	58	-461.72
Nov-2017	-701.08	-5.10	43	-297.30
Dec-2017	-178.42	-1.06	53	-61.78
Jan-2018	-	-	0	-
Feb-2018	-	-	0	-
Mar-2018	-	-	0	-
Apr-2018	-625.24	-6.12	8	-
May-2018	-923.70	-8.38	55	-515.74
Jun-2018	-815.05	-11.80	51	-728.13
Jul-2018	-624.98	-6.50	44	-398.88
Aug-2018	-582.90	-5.27	12	-

4. Discussion

To examine linkages between aquatic FDOM and the terrestrial landscape, Menendez (2017) estimated the normalized difference vegetation index (NDVI) over GCRew wetland using Landsat-8 imagery for 12 acquisitions from November 2014 through January 2016. NDVI can be a proxy for biomass greenness, where yellowed or frost-damaged plants would have lower NDVI (Prabhakara et al., 2015). Maximum NDVI was seen in July, which corresponds to the month of maximum FDOM_{corr} and estimated [DOC]. This suggests that aboveground biomass and marsh plant productivity translates to DOM being mobilized for lateral export. DOC production and transport has been shown to be related to temperature in forested systems, with higher temperatures associated with more dissolution of plant detritus, desorption of sorbed DOC, and more microbial processing (Raymond & Saiers, 2010). Temperature also influences primary production, litter accumulation, and the amount of soil organic matter that is sequestered (Raymond & Saiers, 2010) as demonstrated experimentally at GCRew in a whole-ecosystem (i.e., plant canopy and soil warming to 1.5 m) experiment (Noyce et al., 2019). These biological processes—interactions between plant and microbial activity as they respond to temperature—are driving the seasonality in DOC concentration within the tidal creek yet must be coupled with the seasonality in hydrology to determine export to the Rhode River (Figure 11).

While the high tide concentrations of DOC indicate that there is a “background” estuarine concentration of DOC (i.e., a mixture of degraded terrestrial and biologically derived material), there is strong evidence for the marsh delivering optically and molecularly distinct organic matter to the tidal creek that will ultimately get exported to the sub-estuary. Marsh-derived CDOM from marsh plants and soil leachates has been shown to be of relatively high molecular weight (Tzortziou et al., 2008), and more aromatic and humic in composition than estuarine material. The average exponential slope of CDOM absorption from 290 to 750 nm and $a^*_{CDOM}(300)$ were significantly different between marsh-exported CDOM (low tide) (0.0149 nm⁻¹ and 4.6 m² g⁻¹, respectively) and estuarine CDOM (high tide) (0.0168 nm⁻¹ and 3.6 m² g⁻¹, respectively), demonstrating differences in the quality of marsh-derived versus estuarine CDOM (Tzortziou et al., 2008). Our optical analysis across tides shows consistent tidal controls on CDOM amount and quality with previous studies (Tzortziou et al. [2008]) in this system. The distinct molecular ion differences between low tide and high tide samples at GCRew provide further evidence of GCRew marsh contributions to the tidal creek CDOM and DOC pools. Oxygenated and hydrogen-deficient molecular ions typically correlate well with terrestrially-derived CDOM optical properties (Gonsior et al., 2016; Powers et al., 2021; Wagner et al., 2015), as demonstrated here for the GCRew system. The export of marsh-derived DOM to the Rhode River sub-estuary that is observed at low tide in the GCRew tidal creek, evident by higher $a_{CDOM}(300)$, lower $S_{275-295}$, and oxygenated and hydrogen-deficient molecular ions, supports the Outwelling Hypothesis (Nixon, 1980). Determining the quality of CDOM along with its DOC flux is important to understand the fate of this exported carbon. Non-conservative relationships were previously reported between DOM and salinity in the Rhode River sub-estuary (Tzortziou et al., 2011), suggesting that the GCRew-derived DOM was labile and affected by photochemical and microbial degradation. This was confirmed in incubation experiments by

Logozzo et al. (2021) who found GCRew marsh-exported DOM to be susceptible to photochemical and microbial degradation, with previous light exposure increasing DOM bioavailability.

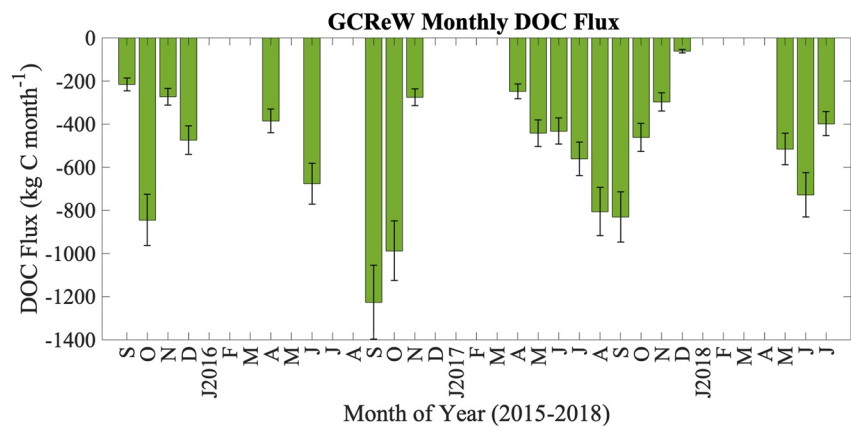


Figure 7. DOC fluxes are shown for months that had 14+ days with continuous measurements from the YSI EXO2, to estimate [DOC], accompanied by Sontek flow data. Fluxes were scaled-up to monthly values based on daily averages. Negative flux values indicate a net export of DOC from the wetland to the sub-estuary.

FDOM_{corr} was the strongest explanatory variable for predicting [DOC] dynamics in this marsh-estuarine system and was found, as expected, to have a positive relationship with DOC concentration, as fluorescent DOM in the 365/480 nm excitation/emission spectral range relates to the colored, humic component of the DOC pool. DO had the second largest standardized coefficient in predicting [DOC] and the coefficient was negative, suggesting that when DO is high, [DOC] is low. This inverse relationship is an example of inverse seasonal and inverse tidal relationships between DO and [DOC] (Nelson et al., 2017). DOC was found to be relatively high in warmer months due to more fresh plant biomass and faster decomposition rates which consumes oxygen. Relatively high DO can also be expected in colder months because of increased DO solubility. DOC concentration has been shown to be high at low tide because of marsh contributions, while DO has been found to be low at low tide because of a drawdown in oxygen in the tidal creek from heterotrophy (Baumann et al., 2014). In addition to metabolic activity within the creek, anoxic porewater drains into the creek at ebb tide when water stage is below bankfull depth (Nelson et al., 2017), and this porewater may also be enriched in DOC, CDOM, and FDOM and depleted in DO relative to surface water (Burdige et al., 2004; Clark et al., 2014). Baumann et al. (2014) reviewed the Outwelling Hypothesis of tidal marsh systems and concluded that *in addition* to their delivery of DOM and nutrients, tidal

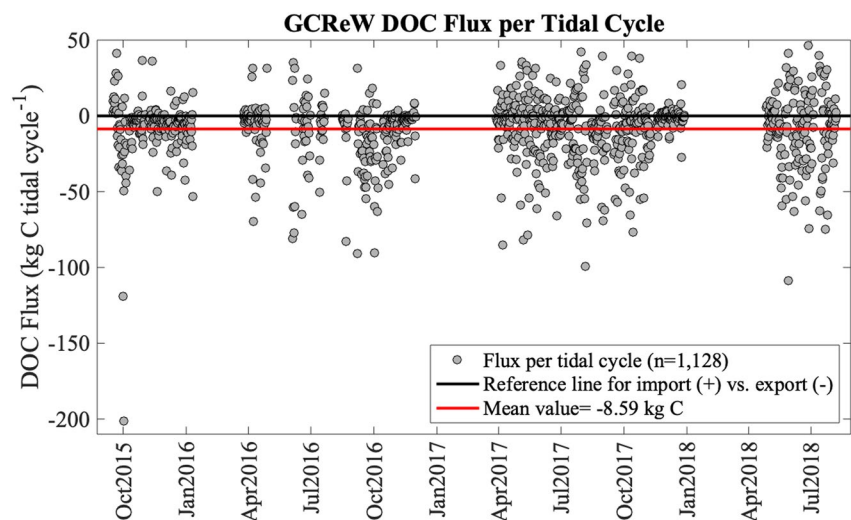


Figure 8. Fluxes of DOC at the GCRew tidal creek are shown per tidal cycle for 1,128 tidal cycles worth of observations from September 2015 to August 2018. Positive values indicate DOC import to the wetland, and negative values indicate wetland DOC export. The mean for these 1,128 tidal cycles is represented by the red line.

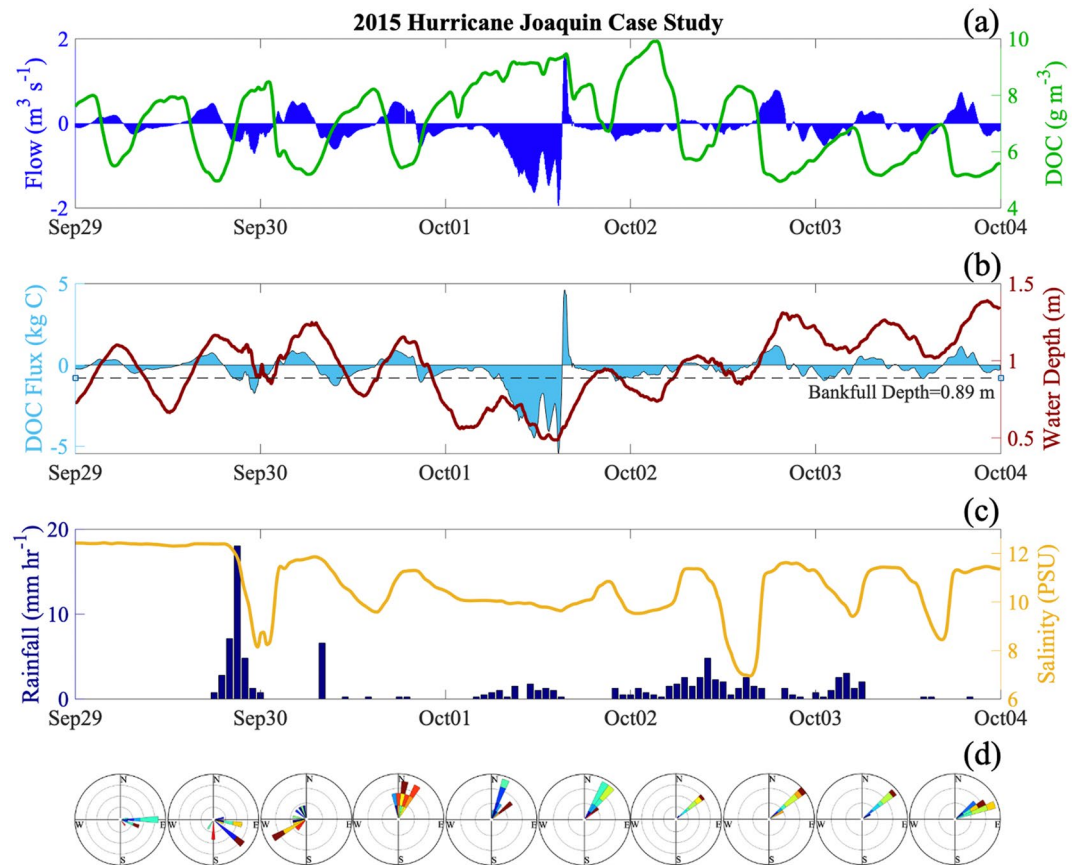


Figure 9. Data from the GCRew tidal creek is shown from September 29 through 3 October 2015. At the top (a), flow in 5-min increments is shown in royal blue along with [DOC] in green. In (b), DOC flux is shown in light blue along with channel water depth (from the Sontek) in red. At panel (c), rainfall in hourly summations is shown in navy along with tidal creek salinity in yellow. On October 1, there was strong export of water from the tidal creek to the sub-estuary, coinciding with depressed water depth within the tidal creek and heightened [DOC]; this all results in a strong DOC flux (export). In panel (d), wind roses indicate shifts in wind direction over 12-hr periods leading up to, during, and after the strong DOC export event.

marshes can contribute hypoxic and acidic water to adjoining water bodies. Our results lend evidence to this relationship for the GCRew system.

Turbidity was the third strongest explanatory variable in the multilinear regression predicting [DOC], with a negative coefficient. $\text{FDOM}_{\text{corr}}$ has already been corrected for the optical attenuation effects of turbidity, thus its entry as a significant variable in the multilinear regression was not due to its corrective impact on FDOM but rather its role as an important water mass marker. Marsh systems are known as sites of particle and associated nutrient deposition (Hook, 1993), leading to low tide, DOC-rich waters often characterized by lower turbidity than adjacent estuarine waters. pH was the fourth strongest explanatory variable in predicting [DOC] in the multilinear regression model, with a positive coefficient, indicating that higher pH corresponded to higher [DOC] within the model. The simple correlation between [DOC] and pH is negative, reflecting the fact that estuarine water entering the creek on rising tides has a higher pH than on falling tides during all seasons. We interpret this pattern as further evidence of DOC-rich marsh porewater draining into the tidal creek at below bankfull depth. DOC from the GCRew marsh has been previously described as enriched in aromatic structures (Tzortziou et al., 2008), which can act as weak acids and bases. Marsh export of porewater (average pH 6.5, Megonigal, per. comm.) combined with benthic and water column respiration in the tidal creek may explain the negative correlation. In building the multilinear regression model, pH maintained a negative coefficient as an explanatory variable for predicting [DOC] except when DO was included, where subsequently the coefficient becomes positive.

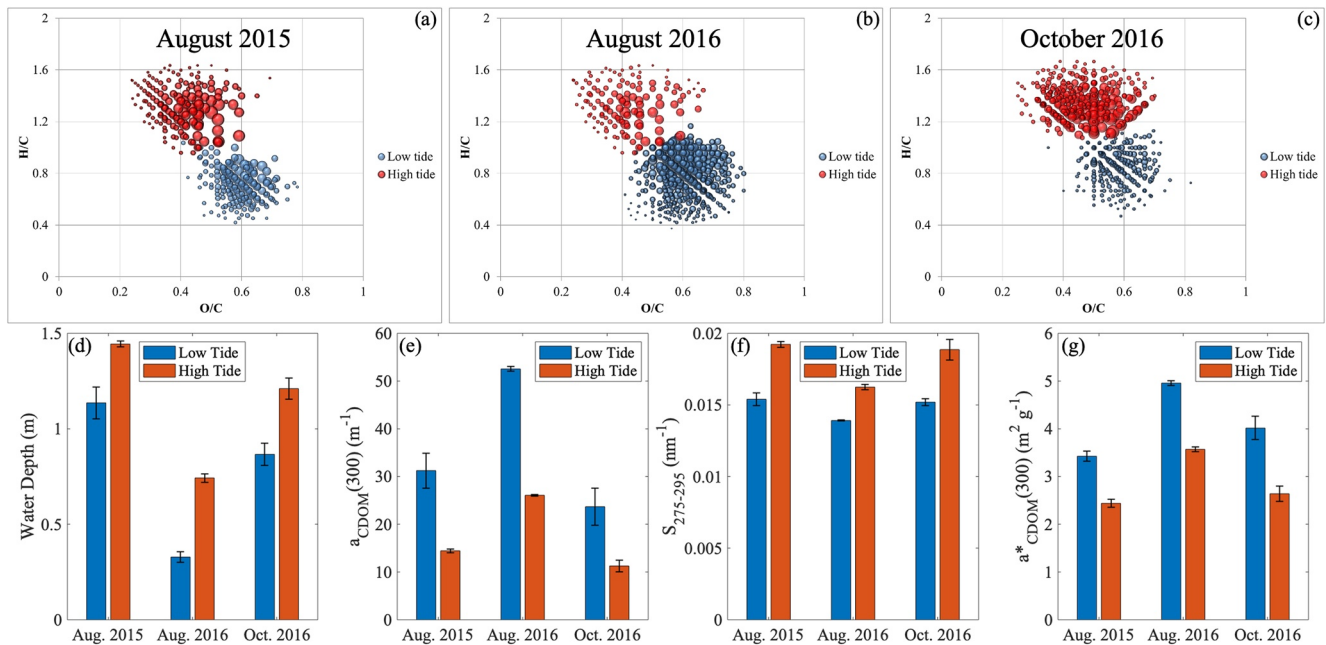


Figure 10. FT-ICR MS data analyzed from within the GCRew tidal creek at low (blue bubbles) versus high tide (red bubbles) for samples collected in August 2015 (a), August 2016 (b), and October 2016 (c). The CHO elements are analyzed above. Low tide samples show a lower ratio of H/C, while a higher ratio of O/C than high tide samples consistently across these 3 months. Plots d-g depict average water depths (from the EXO2, not Sontek) (d), $a_{\text{CDOM}}(300)$ (e), $S_{275-295}$ (f), and $a^*_{\text{CDOM}}(300)$ (g) between low tide (blue, left) and high tide (red, right) samples over the same time period FT-ICR MS samples were collected. For all three months, low tide samples showed higher $a_{\text{CDOM}}(300)$, lower $S_{275-295}$, and higher $a^*_{\text{CDOM}}(300)$ than high tide samples.

Because DO has a similar, but stronger, inverse relationship with [DOC] compared to pH, DO dominates in the full equation, with the positive adjustment for pH refining the relationship.

Salinity was the weakest of the statistically significant explanatory variables in the multilinear regression model to predict [DOC]. The negative coefficient of salinity may reveal information about potential sources of DOC

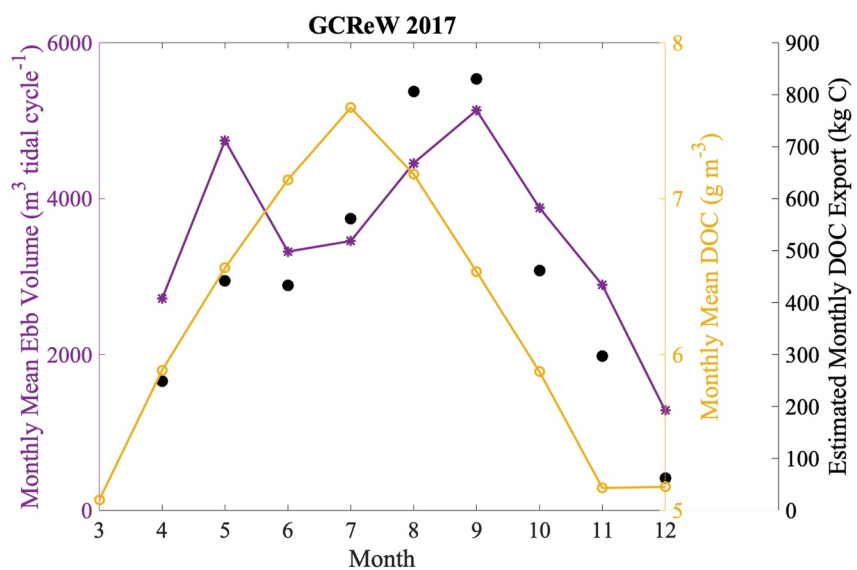


Figure 11. Measurements in 2017 had the best seasonal coverage during this study. For 2017, while DOC (shown in dark yellow with circles) peaks in July, ebb water volume (shown in purple with asterisks) peaks in September (with a second peak in May). The peak in September ebb volume corresponds to the annual peak in estimated monthly DOC flux (shown as black circles).

within the Rhode River sub-estuary. The Susquehanna River is the main freshwater source to the Chesapeake Bay and contributes to strong seasonality in Chesapeake Bay salinity. Susquehanna spring runoff leads to relatively fresh conditions in the Chesapeake Bay from February to May, while the lowest river flow and relatively high salinity occur in late summer through winter (Taft et al., 1980). These trends are reflected in Rhode River sub-estuary seasonal salinity. If the Susquehanna River was the only driver of salinity measured within the tidal creek, the correlation between DOC and salinity should be positive based on their discrete seasonal trends, rather than negative, however Rhode River salinity is also locally affected by Muddy Creek freshwater discharge (location shown in Figure 1). The Muddy Creek watershed was documented as 62% forest, 23% cropland, 12% pasture, and 3% freshwater wetland in 1986 (Jordan & Correll, 1986), so an inverse relationship between [DOC] and salinity within the multilinear regression is likely affected by the Muddy Creek bringing freshwater enriched in organic matter from its watershed. Based on analysis of flow data and salinity data within the tidal creek, freshwater from the upland watershed of GCRW is contributing to the water budget of the marsh tidal creek. Although in most cases salinity at low tide was not statistically significantly different than at high tide, 29% of tidal cycles were found to have low tide water that is fresher than high tide water by 0.5 PSU or more, lending evidence that freshwater is entering the tidal creek either from groundwater or overland GCRW flow. These freshwater inputs may be more apparent at low tide because of the minimum volume of water within the creek at that time, or because the low tide phase facilitates groundwater movement from the marsh interior to the creekbank (Harvey et al., 1987; Howes & Goehring, 1994; Montalto et al., 2006).

Bankfull water depth for the tidal creek is 0.89 m (Nelson et al., 2017), and while this depth threshold was not found to be a clear control on water flux, it is worth considering conceptually, as closing the water balance is essential to fully understanding wetland-estuary DOC exchange. Flooding of the entire marsh system was found to occur approximately once a month during spring tides (Clark et al., 2018). However, based on water fluxes and water depths above bankfull depth, some degree of marsh inundation is happening more frequently, likely due to wind-induced inundation sub-tidally (Clark et al., 2018). As was shown in the 08/30/2017 tidal cycle with highest water import, these high fluxes are associated with high water depths, in this case a high low tide depth (98th percentile) and a high depth at high tide (99th percentile). High tidal creek water depths leading to inundation can result in water pooling on the marsh surface, with this accumulated water lost in the water budget accounting if evapotranspiration occurs, or the water eventually exits as sheet flow to the sub-estuary (i.e., does not exit through the flume). Ebb and flood tide calculations help reveal tidal cycles where water volume is lost to the wetland, or cases of water volume entering the flume from upland or wetland sources. This is consistent with salinity differences between low and high tide water discussed above (i.e., if water was not added or lost within the flume, salinity should remain the same between low and high tide). Continuous monitoring of water flow within a tidal creek can lead to a better understanding of complex tidal marsh hydrology, although inferences still need to be made about external impacts on the flume. Upland freshwater discharge, when present, may be providing an additional terrestrial organic matter source, which is integrated with the marsh organic matter signal during transport to the estuary.

Episodic events can dramatically alter local wind dynamics, precipitation amounts, and extent of marsh inundation, disproportionately affecting water flow and lateral DOC fluxes. In 2011, Hurricane Irene was responsible for 19% of the annual DOC flux exported from a 12-ha forested catchment in the mid-Atlantic Piedmont of the United States (Dhillon & Inamdar, 2013). In 2016, Hurricane Matthew accounted for 25% of annual DOC flux for the Neuse River Estuary, North Carolina, and this material was found to be primarily wetland in origin (Osburn et al., 2019). Using high spatial resolution satellite imagery from Landsat-8/OLI and Sentinel-2/MSI, Cao and Tzortziou (2021) showed that DOC concentrations in the Blackwater National Wildlife Refuge marsh-estuarine system increased by more than a factor of two after the passage of Hurricane Matthew compared to pre-hurricane levels under similar tidal conditions. In this study, just two tidal cycles associated with Hurricane Joaquin in 2015 (representative of ~0.3% of annual tidal cycles) represented over 5% of an annual DOC flux based on GCRW annual estimates. Northerly winds during Hurricane Joaquin contributed to tidal creek water outflow at GCRW as water driven from Muddy Creek and the Rhode River towards the Chesapeake Bay would create a pressure gradient facilitating water and DOC out of the tidal creek (Clark et al., 2018). The Hurricane Joaquin GCRW case study demonstrates the role of precipitation and wind in governing DOC tidal fluxes and provides an example depicting how fluxes can shift quickly in magnitude and direction over subsequent cycles.

A total of 1,128 tidal cycles were analyzed across all seasons and over multiple years, and an average export per tidal cycle was found to be $8.59 (\pm 1.20)$ kg C, with a GCRew DOC flux of $200.66 (\pm 28.09)$ g C m⁻² yr⁻¹. This value falls within the original Childers et al. (2002) literature review that found export ranged between 15 and 328 g C m⁻² yr⁻¹ for 11 systems. It is also very similar to the DOC export of 180.3 g C m⁻² yr⁻¹ reported in Clark et al. (2018) for the same marsh system based on coupled hydrodynamic-biogeochemical model simulations. These DOC flux estimates are considerably higher than previous estimates based on a limited number of tidal cycle observations at GCRew. Jordan et al. (1983) estimated a net DOC export of 43 g C m⁻² yr⁻¹ based on composited low versus high tide samples over 11 tidal cycles, while Tzortziou et al. (2008) found a net export of 32 g C m⁻² yr⁻¹ based on analysis over 9 semi-diurnal tidal cycles with discrete hourly measurements. A major difference between these previous studies and our estimates is the frequency and length of observations. Continuous monitoring of a marsh system, as in this study, allows us to capture the impact of asymmetric tides, seasonal cycles, and extreme events, that all have a major impact on marsh DOC net export at annual timescales. Hurricane Joaquin was a dramatic example of one such event; we posit that many smaller events explain why our estimate of DOC export is higher than previous estimates based on relatively infrequent data. The incorporation of extreme events will become increasingly necessary for accurately quantifying coastal carbon budgets, as their frequency and intensity are predicted to increase (Bender et al., 2010).

5. Conclusion

GCRew has been a site of long-term research, and this study builds upon a strong knowledge base and rich datasets. We demonstrate the utility of an in situ sonde measuring bio-optical and physicochemical water parameters to accurately estimate [DOC] continuously within a wetland tidal creek across seasons and tidal cycles. Paired with concurrent tidal creek water flow data, this estimated [DOC] allowed us to quantify DOC flux for 1,128 tidal cycles over a period from September 2015 to August 2018. We determined the variability in these dynamic biogeochemical exchanges that is impossible to capture with studies based on limited numbers of tidal cycles. We were able to tease apart biogeochemical and physical controls on lateral wetland-estuary DOC flux, revealing that while wetland [DOC] was highest in the tidal creek during summer because of fresh biomass and higher temperature facilitating mobilization, estimated monthly DOC flux was highest in the early fall because of higher water flows. During the episodic event of Hurricane Joaquin, precipitation and wind direction were dominant factors contributing to the largest DOC fluxes seen during this study. The annual lateral DOC export estimated from GCRew to the Rhode River sub-estuary was $200.66 (\pm 28.09)$ g C m⁻² yr⁻¹ and based on NEE reported for GCRew by Erickson et al. (2013) ($+1.5$ and $+1.9$ kg C m⁻² yr⁻¹ for C4 and C3 plant-dominated communities, respectively), between ~11 and 13% of annual carbon sequestered by GCRew could be estimated as lost to lateral flux. Blue Carbon must be examined in the context of lateral carbon export. There is a need to extrapolate local fluxes to the regional and continental scale for use in carbon budgets (Herrmann et al., 2015; Najjar et al., 2018). Improving the accuracy of local system fluxes, as was done in this study at GCRew with continuous monitoring, then in turn improves the accuracy of these aggregated system-wide efforts, which are necessary for carbon cycling modeling and evaluation of future climate change scenarios.

Acknowledgments

The authors would like to thank Andrew Peresta for deployment, maintenance, and calibration of the EXO2 sonde during this project, for laboratory handling of the in situ CDOM and DOC samples, and for many thoughtful discussions surrounding attenuation corrections of EXO2 FDOM measurements. We also would like to thank Gary Peresta for deployment and maintenance of the Sontek during this project duration. This research was supported by National Aeronautics and Space Administration (NASA) grants NNX14AP06 G and NNX14AJ88 G (Carbon Cycle Science Program) and National Science Foundation (NSF) grant 1556556. A.M. was also supported by the National Oceanic and Atmospheric Administration (NOAA) – Cooperative Science Center for Earth System Sciences and Remote Sensing Technologies (CESSRST) under the Cooperative Agreement Grant NA16SEC4810008. A.M. would like to thank the NOAA Educational Partnership Program with Minority Serving Institutions for fellowship support. The statements contained within this manuscript are not the opinions of the funding agency or the U.S. government but reflect the authors' opinions.

Data Availability Statement

Data access: The data used in this study are available in an online repository (<https://doi.org/10.5281/zenodo.6525871>).

References

- Bauer, J. E., Cai, W. J., Raymond, P. A., Bianchi, T. S., Hopkinson, C. S., & Regnier, P. A. G. (2013). The changing carbon cycle of the coastal ocean. *Nature*, *504*(7478), 61–70. <https://doi.org/10.1038/nature12857>
- Baumann, H., Wallace, R. B., Tagliaferri, T., & Gobler, C. J. (2014). Large natural pH, CO₂ and O₂ fluctuations in a temperate tidal salt marsh on diel, seasonal, and interannual time scales. *Estuaries and Coasts*, *38*(1), 220–231. <https://doi.org/10.1007/s12237-014-9800-y>
- Belzile, C., Roesler, C. S., Christensen, J. P., Shakhova, N., & Semiletov, I. (2006). Fluorescence measured using the WETStar DOM fluorometer as a proxy for dissolved matter absorption. *Estuarine, Coastal and Shelf Science*, *67*(3), 441–449. <https://doi.org/10.1016/j.ecss.2005.11.032>
- Bender, M. A., Knutson, T. R., Tuleya, R. E., Sirutis, J. J., Vecchi, G. A., Garner, S. T., & Held, I. M. (2010). Modeled impact of anthropogenic warming on the frequency of intense Atlantic hurricanes. *Science*, *327*(5964), 454–458. <https://doi.org/10.1126/science.1180568>
- Borges, A. V., Delille, B., & Frankignoulle, M. (2005). Budgeting sinks and sources of CO₂ in the coastal ocean: Diversity of ecosystems counts. *Geophysical Research Letters*, *32*(14), 2–5. <https://doi.org/10.1029/2005GL023053>

- Boyd, T. J., & Osburn, C. L. (2004). Changes in CDOM fluorescence from allochthonous and autochthonous sources during tidal mixing and bacterial degradation in two coastal estuaries. *Marine Chemistry*, 89, 189–210. <https://doi.org/10.1016/j.marchem.2004.02.012>
- Bricaud, A., Morel, A., & Prieur, L. (1981). Absorption by dissolved organic matter of the sea (yellow substance) in the UV and visible domains. *Limnology & Oceanography*, 26(1), 43–53. <https://doi.org/10.4319/lo.1981.26.1.0043>
- Bridgman, S. D., Megonigal, J. P., Keller, J. K., Bliss, N. B., & Trettin, C. (2006). The carbon balance of North American wetlands. *Wetlands*, 26(4), 889–916. [https://doi.org/10.1672/0277-5212\(2006\)26\[889:tcbona\]2.0.co;2](https://doi.org/10.1672/0277-5212(2006)26[889:tcbona]2.0.co;2)
- Burdige, D. J., Kline, S. W., & Chen, W. (2004). Fluorescent dissolved organic matter in marine sediment pore waters. *Marine Chemistry*, 89, 289–311. <https://doi.org/10.1016/j.marchem.2004.02.015>
- Cao, F., & Miller, W. L. (2015). A new algorithm to retrieve chromophoric dissolved organic matter (CDOM) absorption spectra in the UV from ocean color. *Journal of Geophysical Research: Oceans*, 120(1), 496–516. <https://doi.org/10.1002/2014jc010241>
- Cao, F., & Tzortziou, M. (2021). Capturing dissolved organic carbon dynamics with Landsat-8 and Sentinel-2 in tidally influenced wetland-estuarine systems. *Science of the Total Environment*, 777. <https://doi.org/10.1016/j.scitotenv.2021.145910>
- Cao, F., Tzortziou, M., Hu, C., Mannino, A., Fichot, C. G., Del Vecchio, R., et al. (2018). Remote sensing retrievals of colored dissolved organic matter and dissolved organic carbon dynamics in North American estuaries and their margins. *Remote Sensing of Environment*, 205, 151–165. <https://doi.org/10.1016/j.rse.2017.11.014>
- Childers, D. L., Day, J. W., & McKellar, H. N. (2002). Twenty more years of marsh and estuarine flux studies: Revisiting Nixon (1980). In M. P. Weinstein, & D. A. Kreeger (Eds.), *Concepts and controversies in tidal marsh ecology* (pp. 391–423). Springer. https://doi.org/10.1007/0-306-47534-0_18
- Clark, C. D., Aiona, P., Keller, J. K., & De Bruyn, W. J. (2014). Optical characterization and distribution of chromophoric dissolved organic matter (CDOM) in soil porewater from a salt marsh ecosystem. *Marine Ecology Progress Series*, 516, 71–83. <https://doi.org/10.3354/meps10833>
- Clark, J. B., Long, W., Tzortziou, M., Neale, P. J., & Hood, R. R. (2018). Wind-driven dissolved organic matter dynamics in a Chesapeake Bay tidal marsh-estuary system. *Estuaries and Coasts*, 41(3), 708–723. <https://doi.org/10.1007/s12237-017-0295-1>
- Del Vecchio, R., & Blough, N. V. (2004). On the origin of the optical properties of humic substances. *Environmental Science and Technology*, 38, 3885–3891. <https://doi.org/10.1021/es049912h>
- Dhillon, G., & Inamdar, S. (2013). Extreme storms and changes in particulate and dissolved organic carbon in runoff: Entering uncharted waters? *Geophysical Research Letters*, 40(7). <https://doi.org/10.1002/grl.50306>
- Dittmar, T., Koch, B., Hertkorn, N., & Kattner, G. (2008). A simple and efficient method for the solid-phase extraction of dissolved organic matter (SPE-DOM) from seawater. *Limnology and Oceanography: Methods*, 6(6), 230–235. <https://doi.org/10.4319/lom.2008.6.230>
- Downing, B. D., Pellerin, B. A., Bergamaschi, B. A., Saraceno, J. F., & Kraus, T. E. C. (2012). Seeing the light: The effects of particles, dissolved materials, and temperature on in situ measurements of DOM fluorescence in rivers and streams. *Limnology and Oceanography: Methods*, 10, 767–775. <https://doi.org/10.4319/lom.2012.10.767>
- Erickson, J. E., Peresta, G., Montovan, K. J., & Drake, B. G. (2013). Direct and indirect effects of elevated atmospheric CO₂ on net ecosystem production in a Chesapeake Bay tidal wetland. *Global Change Biology*, 19(11), 3368–n. <https://doi.org/10.1111/gcb.12316>
- Fellman, J. B., Hood, E., & Spencer, R. G. M. (2010). Fluorescence spectroscopy opens new windows into dissolved organic matter dynamics in freshwater ecosystems: A review. *Limnology & Oceanography*, 55(6), 2452–2462. <https://doi.org/10.4319/lo.2010.55.6.2452>
- Fichot, C. G., & Benner, R. (2011). A novel method to estimate DOC concentrations from CDOM absorption coefficients in coastal waters. *Geophysical Research Letters*, 38(3), 1–5. <https://doi.org/10.1029/2010gl046152>
- Flerus, R., Koch, B. P., Schmitt-Kopplin, P., Witt, M., & Kattner, G. (2011). Molecular level investigation of reactions between dissolved organic matter and extraction solvents using FT-ICR MS. *Marine Chemistry*, 124, 100–107. <https://doi.org/10.1016/j.marchem.2010.12.006>
- Gonsior, M., Valle, J., Schmitt-Kopplin, P., Hertkorn, N., Bastviken, D., Luek, J., et al. (2016). Chemodiversity of dissolved organic matter in the Amazon Basin. *Biogeosciences*, 13(14), 4279–4290. <https://doi.org/10.5194/bg-13-4279-2016>
- Green, S. A., & Blough, N. V. (1994). Optical absorption and fluorescence properties of chromophoric dissolved organic matter in natural waters. *Limnology & Oceanography*, 39(8), 1903–1916. <https://doi.org/10.4319/lo.1994.39.8.1903>
- Hagy, J. D., Boynton, W. R., Keefe, C. W., & Wood, K. V. (2004). Hypoxia in Chesapeake Bay, 1950–2001: Long-term change in relation to nutrient loading and river flow. *Estuaries*, 27(4), 634–658. <https://doi.org/10.1007/BF02907650>
- Harvey, J. W., Germann, P. F., & Odum, W. E. (1987). Geomorphological control of subsurface hydrology in the creekbank zone of tidal marshes. *Estuarine, Coastal and Shelf Science*, 25(6), 677–691. [https://doi.org/10.1016/0272-7714\(87\)90015-1](https://doi.org/10.1016/0272-7714(87)90015-1)
- Helms, J. R., Stubbins, A., Ritchie, J. D., Minor, E. C., Kieber, D. J., & Mopper, K. (2008). Absorption spectral slopes and slope ratios as indicators of molecular weight, source, and photobleaching of chromophoric dissolved organic matter. *Limnology & Oceanography*, 53(3), 955–969. <https://doi.org/10.4319/lo.2008.53.3.0955>
- Henderson, R. K., Baker, A., Murphy, K. R., Hambly, A., Stuetz, R. M., & Khan, S. J. (2009). Fluorescence as a potential monitoring tool for recycled water systems: A review. *Water Research*, 43(4), 863–881. <https://doi.org/10.1016/j.watres.2008.11.027>
- Herrmann, M., Najjar, R. G., Kemp, W. M., Alexander, R. B., Boyer, E. W., Cai, W.-J., et al. (2015). Net ecosystem production and organic carbon balance of U.S. East Coast estuaries: A synthesis approach. *Global Biogeochemical Cycles*, 29, 96–111. <https://doi.org/10.1002/2013GB004736>
- Herzprung, P., Hertkorn, N., Von Tümpling, W., Harir, M., Friese, K., & Schmitt-Kopplin, P. (2014). Understanding molecular formula assignment of Fourier transform ion cyclotron resonance mass spectrometry data of natural organic matter from a chemical point of view. *Analytical and Bioanalytical Chemistry*, 406, 7977–7987. <https://doi.org/10.1007/s00216-014-8249-y>
- Holmquist, J. R., Schile-Beers, L., Buffington, K., Lu, M., Mozdzer, T. J., Riera, J., et al. (2021). Scalability and performance tradeoffs in quantifying relationships between elevation and tidal wetland plant communities. *Marine Ecology Progress Series*, 666, 57–72. <https://doi.org/10.3354/meps13683>
- Hook, D. D. (1993). Wetlands: History, current status, and future. *Environmental Toxicology and Chemistry*, 12(12), 2157–2166. <https://doi.org/10.1002/etc.5620121202>
- Howes, B. L., & Goehring, D. D. (1994). Porewater drainage and dissolved organic carbon and nutrient losses through the intertidal creekbanks of a New England Salt Marsh. *Marine Ecology Progress Series*, 114, 289–301. <https://doi.org/10.3354/meps114289>
- Jordan, T. E., & Correll, D. L. (1986). Flux of particulate matter in the tidal marshes and subtidal shallows of the Rhode River estuary. *Estuaries*, 9(48), 310–319. <https://doi.org/10.2307/1351410>
- Jordan, T. E., & Correll, D. L. (1991). Continuous automated sampling of tidal exchanges of nutrients by brackish marshes. *Estuarine, Coastal and Shelf Science*, 32(6), 527–545. [https://doi.org/10.1016/0272-7714\(91\)90073-k](https://doi.org/10.1016/0272-7714(91)90073-k)
- Jordan, T. E., Correll, D. L., & Whigham, D. F. (1983). Nutrient flux in the Rhode River: Tidal exchange of nutrients by brackish marshes. *Estuarine, Coastal and Shelf Science*, 17, 651–667. [https://doi.org/10.1016/0272-7714\(83\)90032-x](https://doi.org/10.1016/0272-7714(83)90032-x)
- Koch, B. P., Dittmar, T., Witt, M., & Kattner, G. (2007). Fundamentals of molecular formula assignment to ultrahigh resolution mass data of natural organic matter. *Analytical Chemistry*, 79, 1758–1763. <https://doi.org/10.1021/ac061949s>

- Logozzo, L., Tzortziou, M., Neale, P., & Clark, J. B. (2021). Photochemical and microbial degradation of chromophoric dissolved organic matter exported from tidal marshes. *Journal of Geophysical Research: Biogeosciences*, 126(4). <https://doi.org/10.1029/2020jg005744>
- Lucio, M. (2009). Datamining metabolomics: The convergence point of non-target approach and statistical investigation. Thesis, Technische Universität München. Available online at: <http://nbn-resolving.de/urn:nbn:de:bvb:91-diss-20080916-673608-1-4>
- Majidzadeh, H., Uzun, H., Ruecker, A., Miller, D., Vernon, J., Zhang, H., et al. (2017). Extreme flooding mobilized dissolved organic matter from coastal forested wetlands. *Biogeochemistry*, 136, 293–309. <https://doi.org/10.1007/s10533-017-0394-x>
- Mannino, A., Russ, M. E., & Hooker, S. B. (2008). Algorithm development and validation for satellite-derived distributions of DOC and CDOM in the U.S. Middle Atlantic Bight. *Journal of Geophysical Research*, 113(7), 1–19. <https://doi.org/10.1029/2007jc004493>
- Menendez, A. B. (2017). *Temporal variability of fluorescent dissolved organic matter at a brackish, tidal marsh-estuary interface*. MSc Thesis, City University of New York.
- Montalto, F. A., Steenhuis, T. S., & Parlange, J. Y. (2006). The hydrology of Piermont Marsh, a reference for tidal marsh restoration in the Hudson River estuary, New York. *Journal of Hydrology*, 316(1–4), 108–128. <https://doi.org/10.1016/j.jhydrol.2005.03.043>
- Najjar, R. G., Herrmann, M., Alexander, R., Boyer, E. W., Burdige, D. J., Butman, D., et al. (2018). Carbon budget of tidal wetlands, estuaries, and shelf waters of Eastern North America. *Global Biogeochemical Cycles*, 32(3), 389–416. <https://doi.org/10.1002/2017GB005790>
- Nelson, N. G., Muñoz-Carpena, R., Neale, P. J., Tzortziou, M., & Megonigal, J. P. (2017). Temporal variability in the importance of hydrologic, biotic, and climatic descriptors of dissolved oxygen dynamics in a shallow tidal-marsh creek. *Water Resources Research*, 53(8), 7103–7120. <https://doi.org/10.1002/2016WR020196>
- Nixon, S. W. (1980). Between coastal marshes and coastal waters — A review of twenty years of speculation and research on the role of salt marshes in estuarine productivity and water chemistry. In P. Hamilton, & K. B. Macdonald (Eds.), *Estuarine and wetland processes, Marine science* (Vol. 11, pp. 437–525). Springer. https://doi.org/10.1007/978-1-4757-5177-2_20
- Noyce, G. L., Kirwan, M. L., Rich, R. L., & Megonigal, J. P. (2019). Asynchronous nitrogen supply and demand produce nonlinear plant allocation responses to warming and elevated CO₂. *Proceedings of the National Academy of Sciences*, 116(43), 21623–21628. <https://doi.org/10.1073/pnas.1904990116>
- Osburn, C. L., Rudolph, J. C., Paerl, H. W., Hounshell, A. G., & Van Dam, B. R. (2019). Lingering carbon cycle effects of Hurricane Matthew in North Carolina's coastal waters. *Geophysical Research Letters*, 46(5), 2654–2661. <https://doi.org/10.1029/2019GL082014>
- Powers, L. C., Hertkorn, N., McDonald, N., Schmitt-Kopplin, P., Del Vecchio, R., Blough, N. V., & Gonsior, M. (2019). Sargassum sp. act as a large regional source of marine dissolved organic carbon and Polyphenols. *Global Biogeochemical Cycles*, 33(11), 1423–1439. <https://doi.org/10.1029/2019gb006225>
- Powers, L. C., Lapham, L., Malkin, S. Y., Heyes, A., Schmitt-Kopplin, P., & Gonsior, M. (2021). Molecular and optical characterization reveals the preservation and sulfurization of chemically diverse porewater dissolved organic matter in oligohaline and brackish Chesapeake Bay sediments. *Organic Geochemistry*, 161, 104324. <https://doi.org/10.1016/j.orggeochem.2021.104324>
- Prabhakara, K., Dean Hively, W., & McCarty, G. W. (2015). Evaluating the relationship between biomass, percent groundcover and remote sensing indices across six winter cover crop fields in Maryland, United States. *International Journal of Applied Earth Observation and Geoinformation*, 39, 88–102. <https://doi.org/10.1016/j.jag.2015.03.002>
- Raymond, P. A., & Bauer, J. E. (2001). DOC cycling in a temperate estuary: A mass balance approach using natural 14C and 13C isotopes. *Limnology & Oceanography*, 46(3), 655–667. <https://doi.org/10.4319/lo.2001.46.3.0655>
- Raymond, P. A., & Saiers, J. E. (2010). Event controlled DOC export from forested watersheds. *Biogeochemistry*, 100(1), 197–209. <https://doi.org/10.1007/s10533-010-9416-7>
- Regnier, P., Friedlingstein, P., Ciais, P., Mackenzie, F. T., Gruber, N., Janssens, I. A., et al. (2013). Anthropogenic perturbation of the carbon fluxes from land to ocean. *Nature Geoscience*, 6, 597–607. <https://doi.org/10.1038/NNGEO1830>
- Romera-Castillo, C., Sarmento, H., Alvarez-Salgado, X. A. Á., Gasol, J. M., & Marrasé, C. (2011). Net production and consumption of fluorescent colored dissolved organic matter by natural bacterial assemblages growing on marine phytoplankton exudates. *Applied and Environmental Microbiology*, 77(21), 7490–7498. <https://doi.org/10.1128/AEM.00200-11>
- Santos, I. R., Burdige, D. J., Jennerjahn, T. C., Bouillon, S., Cabral, A., Serrano, O., et al. (2021). The renaissance of Odum's outwelling hypothesis in 'Blue Carbon' science. *Estuarine, Coastal and Shelf Science*, 255, 107361. <https://doi.org/10.1016/j.ecss.2021.107361>
- Saraceno, J. F., Pellerin, B. A., Downing, B. D., Boss, E., Bachand, P. A. M., & Bergamaschi, B. A. (2009). High-frequency in situ optical measurements during a storm event: Assessing relationships between dissolved organic matter, sediment concentrations, and hydrologic processes. *Journal of Geophysical Research*, 114(4), 1–11. <https://doi.org/10.1029/2009JG000989>
- Saraceno, J. F., Shanley, J. B., Downing, B. D., & Pellerin, B. A. (2017). Clearing the waters: Evaluating the need for site-specific field fluorescence corrections based on turbidity measurements. *Limnology and Oceanography: Methods*, 15(4), 408–416. <https://doi.org/10.1002/lom3.10175>
- Snyder, L., Potter, J. D., & McDowell, W. H. (2018). An evaluation of nitrate, fDOM, and turbidity sensors in New Hampshire streams. *Water Resources Research*, 54(3), 2466–2479. <https://doi.org/10.1002/2017WR020678>
- Spencer, R. G. M., Butler, K. D., & Aiken, G. R. (2012). Dissolved organic carbon and chromophoric dissolved organic matter properties of rivers in the USA. *Journal of Geophysical Research*, 117(3). <https://doi.org/10.1029/2011JG001928>
- Stedmon, C. A., Markager, S., & Kaas, H. (2000). Optical properties and signatures of chromophoric dissolved organic matter (CDOM) in Danish coastal waters. *Estuarine, Coastal and Shelf Science*, 51(2), 267–278. <https://doi.org/10.1006/ecss.2000.0645>
- Swan, C. M., Nelson, N. B., Siegel, D. A., & Fields, E. A. (2013). A model for remote estimation of ultraviolet absorption by chromophoric dissolved organic matter based on the global distribution of spectral slope. *Remote sensing of environment*, 136, 277–285. <https://doi.org/10.1016/j.rse.2013.05.009>
- Taft, J., Hartwig, E., Loftus, R., & Loftus, R. (1980). Seasonal oxygen depletion in Chesapeake Bay. *Estuaries*, 3(4), 242–247. <https://doi.org/10.2307/1352079>
- Tobias, C., & Neubauer, S. C. (2009). Salt marsh biogeochemistry – An overview. In G. M. E. Perillo, E. Wolanski, D. R. Cahoon, & M. M. Brinson (Eds.), *Coastal wetlands: An integrated ecosystem Approach* (pp. 445–492). Elsevier.
- Tzortziou, M., Neale, P. J., Megonigal, J. P., Pow, C. L., & Butterworth, M. (2011). Spatial gradients in dissolved carbon due to tidal marsh outwelling into a Chesapeake Bay estuary. *Marine Ecology Progress Series*, 426, 41–56. <https://doi.org/10.3354/meps09017>
- Tzortziou, M., Neale, P. J., Osburn, C. L., Megonigal, J. P., Maie, N., & Jaffé, R. (2008). Tidal marshes as a source of optically and chemically distinctive colored dissolved organic matter in the Chesapeake Bay. *Limnology & Oceanography*, 53(1), 148–159. <https://doi.org/10.4319/lo.2008.53.1.0148>
- Tzortziou, M., Zeri, C., Dimitriou, E., Ding, Y., Jaffé, R., Anagnostou, E., et al. (2015). Colored dissolved organic matter dynamics and anthropogenic influences in a major transboundary river and its coastal wetland. *Limnology & Oceanography*, 60(4), 1222–1240. <https://doi.org/10.1002/lno.10092>

- Valle, J., Harir, M., Gonsior, M., Enrich-Prast, A., Schmitt-Kopplin, P., Bastviken, D., & Hertkorn, N. (2020). Molecular differences between water column and sediment pore water SPE-DOM in ten Swedish boreal lakes. *Water Research*, *170*, 115320. <https://doi.org/10.1016/j.watres.2019.115320>
- Van Krevelen, D. W. (1950). Graphical-statistical method for the study of structure and reaction processes of coal. *Fuel*, *29*, 269–284.
- Vodacek, A., Blough, N. V., DeGrandpre, M. D., Peltzer, E. T., & Nelson, R. K. (1997). Seasonal variation of CDOM and DOC in the Middle Atlantic bight: Terrestrial inputs and photooxidation. *Limnology & Oceanography*, *42*(4), 674–686. <https://doi.org/10.4319/lo.1997.42.4.0674>
- Wagner, S., Jaffé, R., Cawley, K., Dittmar, T., & Stubbins, A. (2015). Associations between the molecular and optical properties of dissolved organic matter in the Florida Everglades, a model coastal wetland system. *Frontiers of Chemistry*, *3*. <https://doi.org/10.3389/fchem.2015.00066>
- Ward, N. D., Bianchi, T. S., Medeiros, P. M., Seidel, M., Richey, J. E., Keil, R. G., & Sawakuchi, H. O. (2017). Where carbon goes when water flows: Carbon cycling across the aquatic continuum. *Frontiers in Marine Science*, *4*. <https://doi.org/10.3389/fmars.2017.00007>
- Watras, C. J., Hanson, P. C., Stacy, T. L., Morrison, K. M., Mather, J., Hu, Y. H., & Milewski, P. (2011). A temperature compensation method for CDOM fluorescence sensors in freshwater. *Limnology and Oceanography: Methods*, *9*, 296–301. <https://doi.org/10.4319/lom.2011.9.296>